

Main Ethiopian Rift landslides formed in contrasting geological settings and climatic conditions

Karel Martínek*^{1, 2}, Kryštof Verner^{2, 3}, Tomáš Hroch², Leta A. Megerssa^{3, 2}, Veronika Kopačková², David Buriánek², Ameha Muluneh⁴, Radka Kalinová³, Miheret Yakob⁵, Muluken Kassa⁴

*corresponding author

¹ *Institute of Geology and Palaeontology, Faculty of Science, Charles University, Albertov 6, Prague, 12843, Czech Republic (karel.j.martinek@gmail.com)*

² *Czech Geological Survey, Klárov 3, 118 21 Prague, Czech Republic*

³ *Institute of Petrology and Structural Geology, Faculty of Science, Charles University, Albertov 6, Prague, 12843, Czech Republic*

⁴ *School of Earth Sciences, Addis Ababa University, Arat Kilo, 1176, Addis Ababa, Ethiopia*

⁵ *Geological Survey of Ethiopia, CMC road, Bole Keb.10/Wor.6, POBox: 2302, Addis Ababa, Ethiopia*

Abstract. The Main Ethiopian Rift (MER), where active continental rifting creates specific conditions for landslide formation, provides a prospective area to study the influence of tectonics, lithology, geomorphology, and climate on landslide formation. New structural and morphotectonic data from CMER and SMER support a model of progressive change in the regional extension from NW – SE to the recent E(ENE) – W(WSW) direction driven by the African and Somalian plates moving apart with the presumed contribution of the NNE(NE) – SSW(SW) extension controlled by the Arabic Plate. The formation and polyphase reactivation of faults in the changing regional stress-field significantly increase the rocks' tectonic anisotropy, slope and the risk of slope instabilities forming. According to geostatistical analysis landslides in the central and southern MER occur on steep slopes, almost exclusively formed on active normal fault escarpments. Landslides are also influenced by higher annual precipitation, precipitation seasonality, vegetation density and seasonality. Deforestation is also important predisposition, because rockfalls and landslides typically occur on areas with bushland, grassland and cultivated landcover.

A detailed study on active rift escarpment in the Arba Minch area revealed similar affinities as in regional study of MER. Landslides here are closely associated with steep, mostly faulted, slopes and a higher density of vegetation. Active faulting forming steep slopes is the main predisposition for landslide formation here, and the main triggers are seismicity and seasonal precipitation. The Mejo area situated on the uplifting Ethiopian Plateau 60 km east of the Rift Valley shows that landslide occurrence is strongly influenced by steep erosional slopes and deeply weathered Proterozoic metamorphic basement. Regional uplift accompanied by rapid head-ward erosion forming steep slopes together with unfavourable lithological conditions is the main predisposition for landslide formation, the main triggers are intense precipitation and higher precipitation seasonality.

Keywords:

Landslides, Main Ethiopian Rift (MER), morphotectonics, tectonics, geological setting, climate, geostatistics

1. Introduction

Slope instabilities including mainly landslides, rockfalls and debris flows are usually influenced by key factors such as slope, bedrock lithology and rock fabric anisotropy, active tectonics and seismicity, type and grade of weathering, climatic conditions, vegetation cover, land use and human activity. Links between these factors and the formation of landslides and rockfalls are complex (e.g., Abebe et al., 2010; Meinhardt et al., 2015). Geomorphic indices have been used to decipher links between landform and tectonics in several studies (Ayalew and Yamagishi, 2004; Ayalew et al., 2004). However, the influence of other factors on slope instabilities is unclear and a matter of current debate (e.g., Asfaw, 2007; Temesgen et al., 1999; Vařilová et al., 2015; Woldearegay, 2013). In general, ongoing discussions on the formation of slope instabilities in an active rift setting state either tectonics, climate or anthropogenic activity as triggering factors depending on the characteristic conditions at the particular locality (e.g., Mancini et al., 2010; Peduzzi, 2010; Wotchoko et al., 2016). Other studies also conclude that lithology and precipitation are the main landslide controlling factors (e.g., Kumar et al. 2019; and references therein). Geomorphic indices, such as slope, aspect, hypsometric integral, the stream length gradient index or river incision rates, are

53 capable of detecting landform responses to tectonics (Ayalew and Yamagishi, 2004; Gao et al., 2013) but studies
54 showing slope instabilities having a direct link to active tectonics are relatively rare (Chang et al., 2018 and
55 references therein). Other studies also conclude that lithology and precipitation are main landslide controlling factors
56 (e.g., Kumar et al. 2019 and references therein).

57 Central and southern parts of the Main Ethiopian Rift (MER), which belong to the northern part of the East African
58 Rift System (EARS), form a relatively narrow, slowly spreading extensional zone with a humid, strongly seasonal
59 climate. The rift valley is significantly drier in comparison to more humid rift flanks and plateau. There is a thick
60 sequence of unconsolidated, often strongly weathered volcanoclastic deposits cropping out in grabens, on steep
61 tectonic slopes or occasionally also on moderately elevated areas. Such a complex environment is an excellent
62 natural laboratory to study the interplay of factors influencing various types of slope instabilities as they form in
63 different geological and geomorphic conditions. Active extensional tectonism has a strong influence on the present-
64 day morphology, but there are also important variations in climatic parameters (annual precipitation, seasonality);
65 moreover, a population explosion in the last decades has led to extensive deforestation, overgrazing and dramatic
66 changes of landcover and land use, which all may have significant importance in landslide formation (FAO 2001;
67 Janetos and Justice, 2000; Gessesse, 2007; Gete and Hurni, 2001; Melese 2016).

68 This multidisciplinary study is focused on evaluating the landslide distribution in the central and southern MER. A
69 combination of the results of geological, geohazard and structural mapping, with remotely sensed data, and climatic,
70 vegetation and land use indicators is assessed using geostatistical methods. The discussion of the main factors
71 influencing the formation of landslides in the regional scale in the central and southern MER and also on a detailed
72 scale in the Mejo and Arba Minch areas in the southern part of the MER is the main focus of this study. In regional
73 scale study the direct link to tectonics is clear, so we present large dataset of new field structural data from this area.
74 The situation in detailed scale studies in Mejo and Arba Minch is more complex. These two areas have contrasting
75 styles of tectonic setting and varying lithological and climatic conditions: the Mejo landslide area is more humid,
76 located on the eastern plateau, 60 km east of the rift valley and dominated by highly weathered Proterozoic
77 basement rocks, while the Arba Minch landslide area is situated directly on the western rift escarpment with active
78 tectonism and seismicity, and dominated by Tertiary volcanic rocks (Fig. 1). In both areas, slope failures are closely
79 associated with steep slopes, but these are generated by very different processes – either active rift normal faulting
80 or deep head-ward river erosion of uplifting rift flank. The anthropogenic influence is also discussed, but only
81 locally, because the relevant data for a thorough geostatistical evaluation are unfortunately missing.

82

83 **2. Geological and geohazard setting**

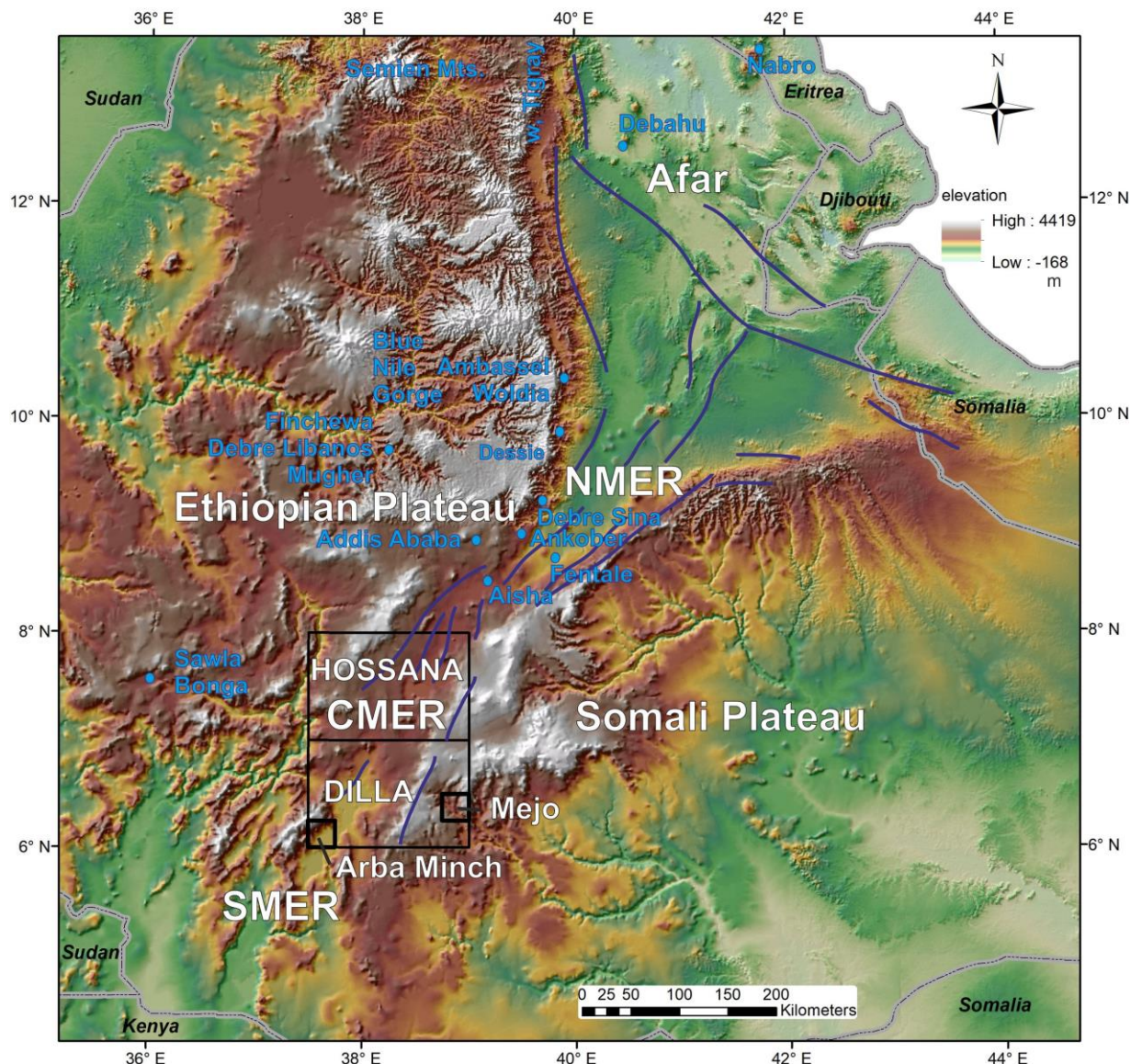
84 **2.1. Geology and tectonics of the studied area**

85 The overall geological pattern of the southern Ethiopia includes a basement formed by metamorphic rocks of the
86 Neoproterozoic age, which have been overlaid by widespread volcanic sequences ranging from pre-rift Cenozoic
87 volcanism to the Main Ethiopian Rift (MER) associated volcanism (Bonini et al., 2005; Hayward and Ebinger, 1996;
88 Woldegabriel et al., 2000). The Precambrian rocks exposed in southern Ethiopia constitute the most southern part of
89 the Arabian-Nubian Shield (ANS) which includes several terrane assemblages (for a review see Fritz et al. 2013 and
90 references therein). The ANS is an assemblage of juvenile low-grade volcano-sedimentary rocks and associated
91 plutons and ophiolite traces with ages between ~890 and 580 Ma (Fritz et al., 2013). The Main Ethiopian Rift
92 (MER) is an active intra-continental rift bearing magma-dominated extension of the African (Nubian), Somalian,
93 and Arabian lithospheric plates (e.g., Acocella, 2010; Agostini et al., 2011). Three segments of the MER reflecting
94 temporally and spatially different stages of regional extension and volcanic activity have been defined (e.g. Hayward
95 and Ebinger, 1996; Muluneh et al., 2014): (a) the Northern Main Ethiopian Rift (NMER), (b) the Central Main
96 Ethiopian Rift (CMER) and (c) the Southern Main Ethiopian Rift (SMER, see Fig. 1). In the southern part of the
97 MER, the current rate of ~E – W oriented extension between the African and Somalian plates amounts 5.2±0.9
98 mm/yr (Saria et al., 2014).

99 The volcanic activity in the studied parts of the CMER (Hossana Area) and SMER (Dilla Area) could be divided
100 into three major episodes (Bonini et al., 2005; Corti, 2009; Hayward and Ebinger, 1996). The Eocene to Oligocene
101 pre-rift volcanic products (~45 to 27 Ma) comprise mainly tholeiite to alkaline basalt lava flows and the associated
102 volcanoclastic deposits (Amaro-Gamo Basalts) with the presence of rhyolite ignimbrites (Shole Ignimbrites) and
103 minor trachytes (Burianek et al., 2018; Verner et al., 2018b; Verner et al., 2018d). The Miocene syn-rift volcanic
104 products (~22 to 8 Ma) are represented by basalts, felsic volcanites and volcanoclastic rocks (rhyolite lava, minor
105 ignimbrites, trachyte lava flows and related pyroclastic deposits) belonging mainly to the Getra and Kele sequences
106 including Mimo trachyte (Bonini et al., 2005; Ebinger et al., 1993; Ebinger et al., 2000). These two events were

107 followed by a period of drastically low volcanism except for a small eruption of peralkaline pantelleritic ignimbrites
 108 intercalated with minor basaltic lava flows in the areas beyond the rift escarpments (Bonini et al., 2005; see also Fig.
 109 4). Subsequently, the products of Pleistocene to Holocene post-rift volcanic activity (~1.6 – 0.5 Ma) are bi-modal
 110 volcanites and volcanoclastic rocks such as, for example, massive Nech-Sar basalts, rhyolites, strongly welded
 111 rhyolitic ignimbrites and other pyroclastic deposits (Ebinger et al., 1993). A typical example of post-rift volcanic
 112 activity in the southern CMER is the lower Pleistocene formation of unconsolidated pyroclastic deposits on the rift
 113 floor (e.g., Corbetti Volcanic System, Rappich et al., 2014), which was consequently disturbed by tectonic
 114 movements and erosion.

115 The complex fault pattern of the MER (interference of SSW(SW) -NNE(NE), N-S and WNW(W) -ESE(E) trending
 116 faults) has been attributed to various mechanisms of contrasting hypothesis (for a review see Abate et al., 2015;
 117 Erbello and Kidane, 2018): (a) The pure extension orthogonal to the rift; (b) a right-lateral NW – SE to the NNW –
 118 ESE transtension continuously transferred to sinistral oblique rifting as a result of an E – W regional extension; (c) a
 119 constant NE(ENE) – SW(WSW) trending extension; (d) constant extension in the NW – SE direction and (e)
 120 constant E – W to ESE – WNW extension.
 121



122
 123 *Fig. 1 The Hossana and Dilla areas in the central and southern part of the Main Ethiopian Rift (MER). The location*
 124 *of the NMER (northern MER), CMER (central MER), SMER (southern MER) and Mejo and Arba Minch case study*
 125 *areas are also indicated. The blue lines represent major fault zones. Digital elevation models AsterDEM and*
 126 *SRTM3 with resolution 30 m were used.*
 127

2.2. Geohazards in the central and southern MER

Active extensional tectonics and the intense volcanism associated with the East African Rift System (e.g., Agostini et al., 2011; Chorowicz, 2005) represent one of the main reasons for frequent hazardous geological phenomena in the Main Ethiopian Rift (MER). Characteristic rift-related morphology, seasonal climatic conditions and inappropriate human interference in the landscape create suitable conditions for hazardous geological processes. Endogenous risk factors such as earthquakes, volcanism and post-volcanic phenomena are closely related with tectonics in this area. The geomorphology is highly variable across the MER and is mainly the result of volcanic and tectonic events with the associated erosional and depositional processes (Billi, 2015).

Notable geohazard features across and along the MER range from intense erosion to slope instability-related mass wasting processes including rock falls, debris flows up to shallow and deep-seated landslides, all with immense costs in terms of casualty and infrastructure loss (Abebe et al., 2005; Ayalew, 1999; Hearn, 2018). Landslides are rather more common in the highlands of Ethiopia. The most affected regions are the Blue Nile Gorge (Ayalew and Yamagishi, 2004; Gezahegn and Dessie, 1994; JICA and GSE, 2012; Tadesse, 1993), the Dessie area and the highlands surrounding Ambassel and Woldia (Ayenew and Barbieri, 2005; Fubelli et al., 2008), the Semien highlands, particularly western and central Tigray, the Sawla and Bonga areas of south Ethiopia (Lemessa et al., 2000) and the MER margins of the western and eastern escarpment (Kycl et al., 2017; Rapprich and Eshetu, 2014; Rapprich et al., 2014; Temesgen et al., 2001), the surroundings of Finchewa and the Debre Libanos and the Muger locality (Zvelebil et al., 2010). On the western escarpment of the MER, a vast and recurrent landslide is notable close to the town of Debre Sina at the locality of Yizeba Weyn in central Ethiopia (Kropáček et al., 2015).

Other common geological hazards that recurrently appear in the area are ground fissures in various sectors along the rift floor. For example, north of the Fentale area in the northern MER (Williams et al., 2004) and various localities in the central MER segment (Asfaw, 1982; Asfaw, 1998; Ayalew et al., 2004) which often transform into deep and long gully systems (Billi and Dramis, 2003). Persistent seismic tremors, usually of lower magnitudes, are apparently located in the entire rift floor (e.g., Wilks et al., 2017). Particular clusters and source zones have been identified in Ethiopia those being (1) the western plateau margin, (2) the central Afar, (3) the Aisha block, (4) the Ankober area, (5) the central Main Ethiopian Rift and (6) the southwestern Main Ethiopian Rift (Ayele, 2017). Nevertheless, historical high magnitude earthquake records have also been reported (Asfaw, 1992; Gouin, 1975; Gouin, 1979; Wilks et al., 2017). An updated probabilistic seismic hazard analysis and zonation has since been recently carried out with seismotectonic source zones constrained from recent studies for the Horn of Africa with reference to the East African Rift Valley (Ayele, 2017).

In addition to the seismic tremors, volcanism is also of apparent risk. Among the recent events are the Nabro Volcano in 2011 in the far northern part of the Afar triangle (Goitom et al., 2015) and the Debahu rifting and volcanic dyke swarm intrusion events in 2005 (Ayele et al., 2007; Ayele et al., 2009). These two events each triggered major alarms significant enough to warrant flight diversions (in the case of the Nabro Volcano) across the region and the temporary displacement of local people (e.g., Goitom et al., 2015).

3. Methods and data

Field geological, structural, geomorphological and engineering geological mapping were conducted to acquire geological, tectonic, geomorphological and rock mechanic properties (rock mass strength) characteristics.

Geotechnical data

Rock mass strength is obtained from the Engineering geological map of Hossana map sheet (Yekoye et al., 2012) and Dilla map sheet (Habtamu et al., 2012). The maps are prepared based on extensive and multiple types of field data to classify the lithological units into ranks of strength class as Very Low, Low, Medium, High, Very High rock mass strength units. These classifications are based on multiple criteria evaluations determined from field documentation including intact rock strength, discontinuity conditions and degree of weathering. The intact rock strength determination is made either by Schmidt hammers or testing of representative irregular samples under the point load tester and the results normalized to standard size of sample as recommended by ISRM (1985) to IS_{50} reference strength. The discontinuity condition is determined by considering the spacing, aperture and discontinuity surface roughness and overall geometry. The degree of weathering on the other hand is determined qualitatively on the bases of the criteria set out in British Standard (BS 5930, 1981) from various outcrops in the region.

Climatic data

181 The precipitation data were obtained from the national database that was set up by the Centre for Development and
182 Environment (CDE), University of Bern, Switzerland in the 1990's for all of Ethiopia. Since its beginning, the
183 dataset has been upgraded with additional information layers but the dataset released as version I on a single CD-
184 ROM, which has mean monthly precipitation data of the major settlement areas with information on the temporal
185 coverage of recorded years, has been used in this study (CDE, 1999). Precipitation point data (Centre for
186 Development and Environment, 1999) were averaged (annual, each month) and then the spatial distribution over the
187 areas of interest were interpolated using the Inverse Distance Weighted method (IDW). Nevertheless, the
188 precipitation seasonality index could not be calculated due to data inhomogeneities, where only some stations have a
189 recording period of more than 20 yrs., but often less than 5 yrs. In order to calculate a seasonality index, 30 yrs.
190 continuity is required. Therefore, precipitation seasonality was evaluated using standard deviation among particular
191 monthly precipitations and by wet (July + August) and dry season (December + January) differences. Monthly
192 averages of all available data were considered for calculations.

193

194 **Remote sensing data and morphotectonic analysis**

195 Aster DEM, SRTM3 and Landsat 7 ETM+ were used for morphotectonic analysis, the vegetation index (NDVI)
196 based on Modis (Terra Modis, USGS eMODIS Africa 10-Day Composite) and land use / land cover data available
197 from the U.S. Geological Survey (<https://earthexplorer.usgs.gov/>, 2018) were also evaluated. Modis scenes from
198 January (peak of dry season) and August (peak of wet season) 2016 were used for the vegetation assessment.
199 The main approach for the morphotectonic analysis followed that used by Dhont and Chorowicz (2006 and
200 references therein). The main aim was to use DEM imagery to interpret the largest neotectonic structures in the
201 central and southern MER regions. Single-directional and multi-directional shaded reliefs and an elevation-coloured
202 ASTER DEM image (Fig. 3) was generated using ArcMap 10.6 (www.esri.com). This DEM constitutes the basis for
203 morphotectonic analysis at the regional scale. The faults mapped can be considered as the main neotectonic faults
204 because they have a prominent expression in the morphology. In some cases, they form asymmetric ranges with one
205 side corresponding to breaks in slope or scarps; by the displacement of Pleistocene and Neogene lithological
206 boundaries; by the occurrence of straight lines of kilometres to several tens of kilometres in length. The images were
207 compared with field geological mapping data to distinguish the scarps formed by active faults from those formed by
208 differential erosion of contrasted lithology.

209 The emplacement of volcanoes, which are abundant in study area, can also be related to tectonic structures such as
210 tension fractures or open faults. Small volcanoes arranged along the straight lines or linear clusters of adjacent
211 volcanoes were also interpreted as linear structures. The result of the interpretation is called "linear indices" which
212 mostly represent active faults (normal and normal-oblique slip), but because of uncertainties in detailed lithology in
213 some areas and a lack of field verification in some cases, the "linear indices" may also represent prominent fracture
214 zones, in exceptional cases, also lithological boundaries. To avoid such uncertainties, an independent evaluation of
215 the geomorphology by numerical methods was carried out. For an evaluation of the main tectonic indications of the
216 CMER and SMER, morphotectonic analysis was carried out at a regional scale of 1: 250 000 (presented in sections
217 4.1. and 4.4.), while case studies Mejo and Arba Minch were evaluated on a detailed scale of 1: 50 000 (chapter
218 4.5.). "Linear indices" are referred as "lineaments" further in the text and figures.

219 In addition to a visual interpretation of linear indices, a quantitative technique - morphometry - was also employed
220 to analyse landforms in a quantitative manner. This technique uses numerical parameters such as slope, surface
221 curvature and convexity to extract morphological and hydrological objects (e.g., stream networks, landforms) from
222 DEM (Fisher et al., 2004; Pike, 2000; Wood, 1996). Landforms and lithological units reflect also different
223 geotechnical properties (e.g., rock strength, degree of weathering) so they can be identified by these numerical
224 methods. Various studies have been carried out to link morphometry with fluvial erosion, tectonics and diverse
225 geomorphological conditions and volcanic activity (Altin and Altin, 2011; Bolongaro-Crevenna et al., 2005; Ganas
226 et al., 2005; Kopačková et al., 2011; Rappich et al., 2010). Morphometric maps were constructed utilizing Wood's
227 algorithm based on SRTM DEM data (30 m pixel resolution). First, the topographic slope and the maximum and
228 minimum convexity values were derived at a pixel-by-pixel basis. The variation in these parameters was quantified
229 for each pixel with respect to neighbouring pixels (in orthogonal directions). Secondly, based on a set of tolerance
230 rules, morphometric classes were defined for each pixel: ridge, channel, plane, peak, pit and pass (Wood, 1996).
231 Wood's algorithm allows the relief to be parametrized by setting different values for the tolerance of the topographic
232 slope and convexity. In this study the slope tolerance of 3.0 and convexity tolerance of 0.02 were used for the best
233 fit.

234

235 **4. Results and interpretations**

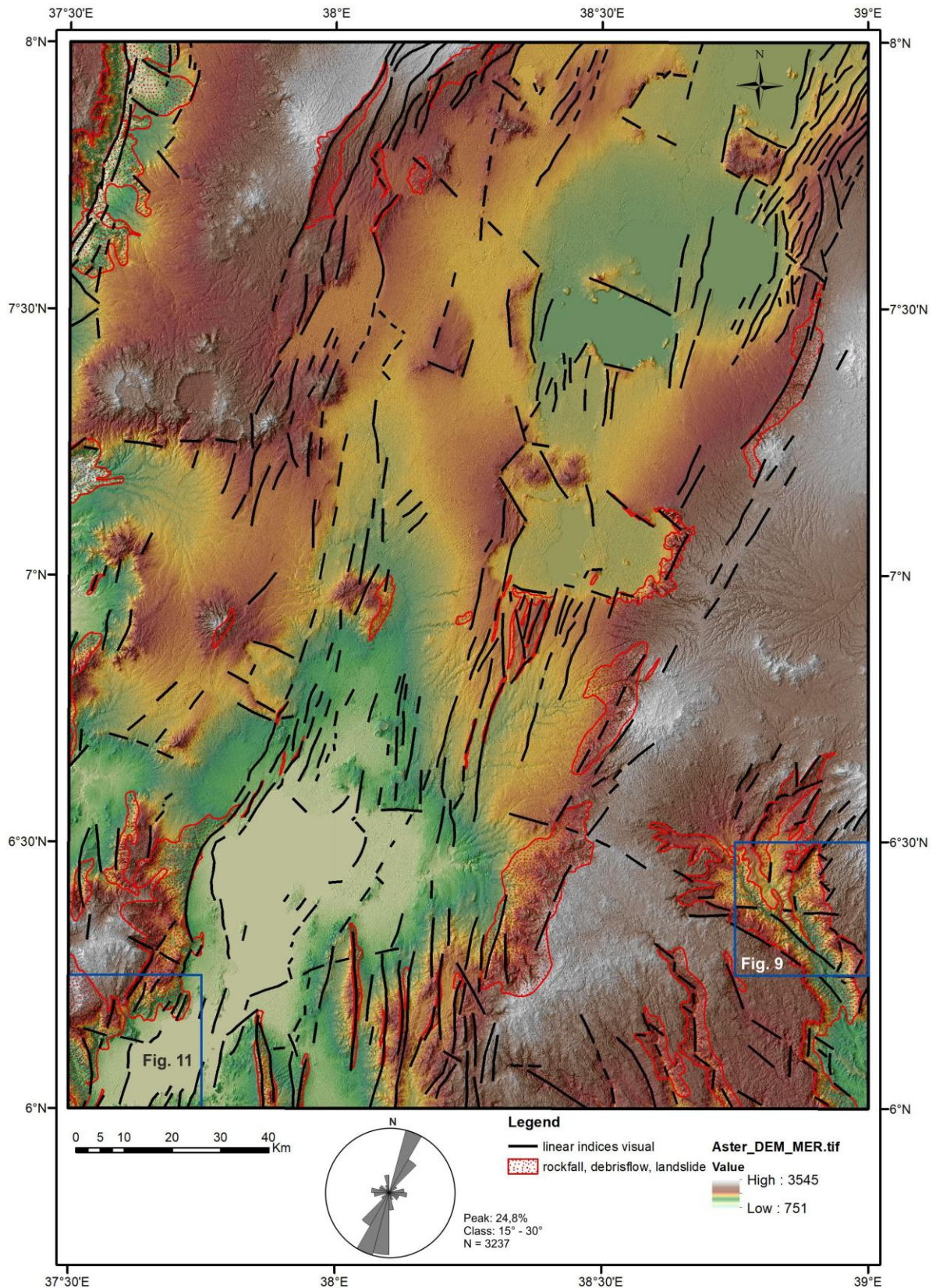
236 The results of the regional study of morphotectonics, morphometric and field structural analysis, slope failure
237 mapping and a geostatistical evaluation of the relationships between tectonic, lithological and surface conditions,
238 and the occurrence of the landslides are presented here. Also, a more detailed evaluation is finally carried out taking
239 two case study sites at Mejo (on MER eastern shoulder) and Arba Minch (western MER escarpment) areas which
240 have a contrasting geological and climatic setting across the MER.

241
242

243 **4.1. Morphotectonic and morphometric analysis**

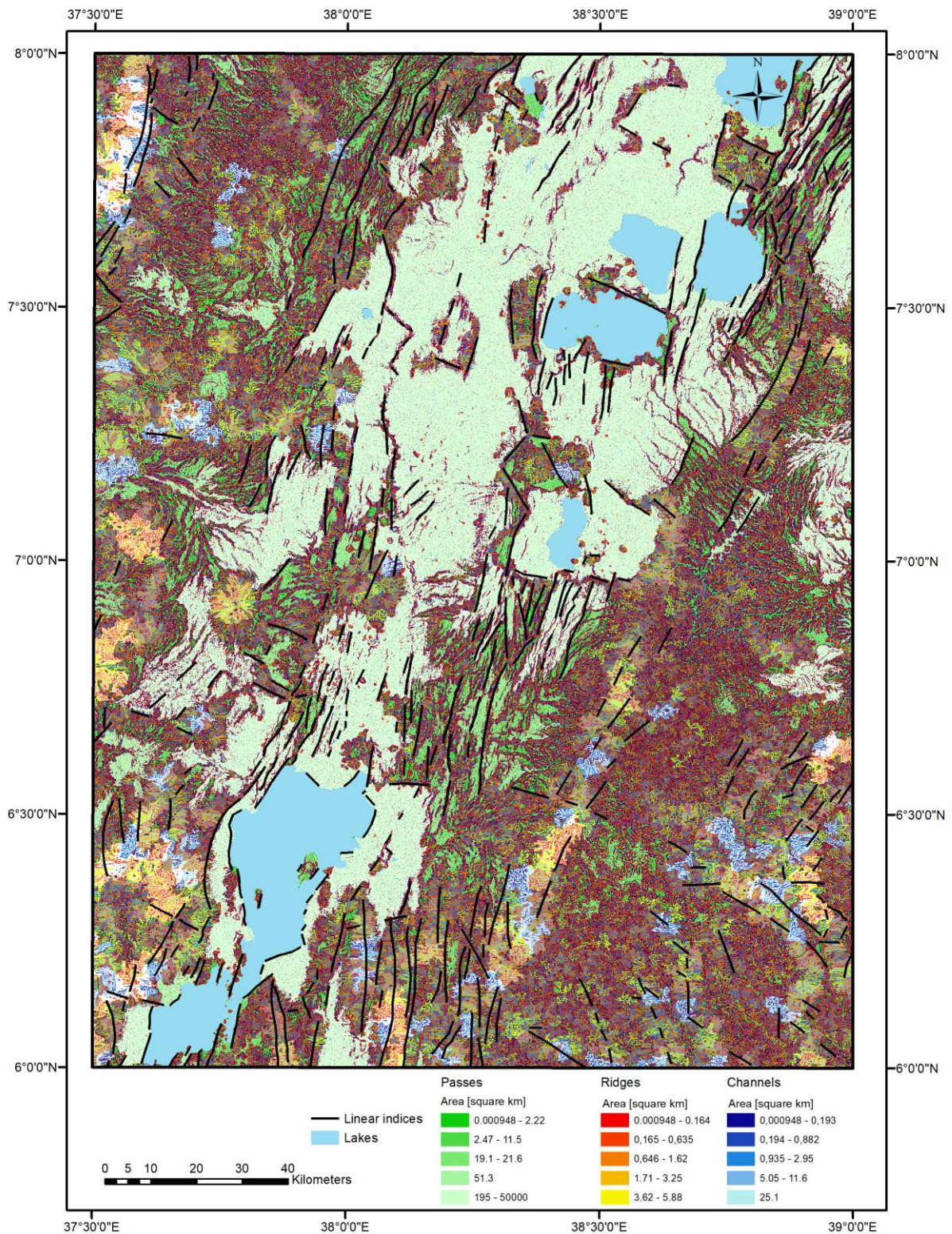
244 Shaded relief maps, derived from DEMs with NW, N and NE illumination, and multidirectional shaded relief maps
245 were used as a base map for morphotectonic interpretation. After carrying out the first stage of a visual interpretation
246 of the lineaments, the second stage was carried out on the automated/numerical morphology base map, which helped
247 uncover some important lineaments with a not so prominent morphological expression. Based on a comparison with
248 geological maps, lineaments representing lithological boundaries, without evidence of faults, were removed during
249 the third stage. Thus, the interpreted lineaments mostly represent present-day active faults, fault zones, important
250 fracture zones and possibly also shear zones (if there are any) which are manifested in morphology. Moreover, older
251 faults with a prominent lithological contrast can be expressed in morphology. The interpretation was made on a
252 scale of 1:250 000, so only the lineaments considered to represent a main fault or other tectonic zones have been
253 mapped.

254



255
 256 *Fig. 2. DEM (colour elevation map on multidirectional shaded relief) of the Dilla and Hossana areas with visually*
 257 *interpreted linear indices and the distribution of their strikes in a rose diagram. The location of the Mejo (Fig. 9)*
 258 *and Arba Minch (Fig. 11) detailed study areas are also shown (see section 4.5).*
 259

260 A combination of a visual morphotectonic interpretation based on DEMs (Fig. 2) and an interpretation on
261 morphometric landforms (Fig. 3) was used to map lineaments. The study area is characterised by a predominance of
262 NNE-SSW oriented lineaments mostly representing the major normal faults of the rift valley. The central and
263 northern parts of the study area represent a relatively wider rift zone with extension spread over a larger area, while
264 the southern part is narrower with steeper topographic gradients and more prominent vertical displacements on the
265 faults. The subordinate population of lineaments, mostly perpendicular to the strike of the rift has E-W to WNW
266 trend showing also vertical displacement.

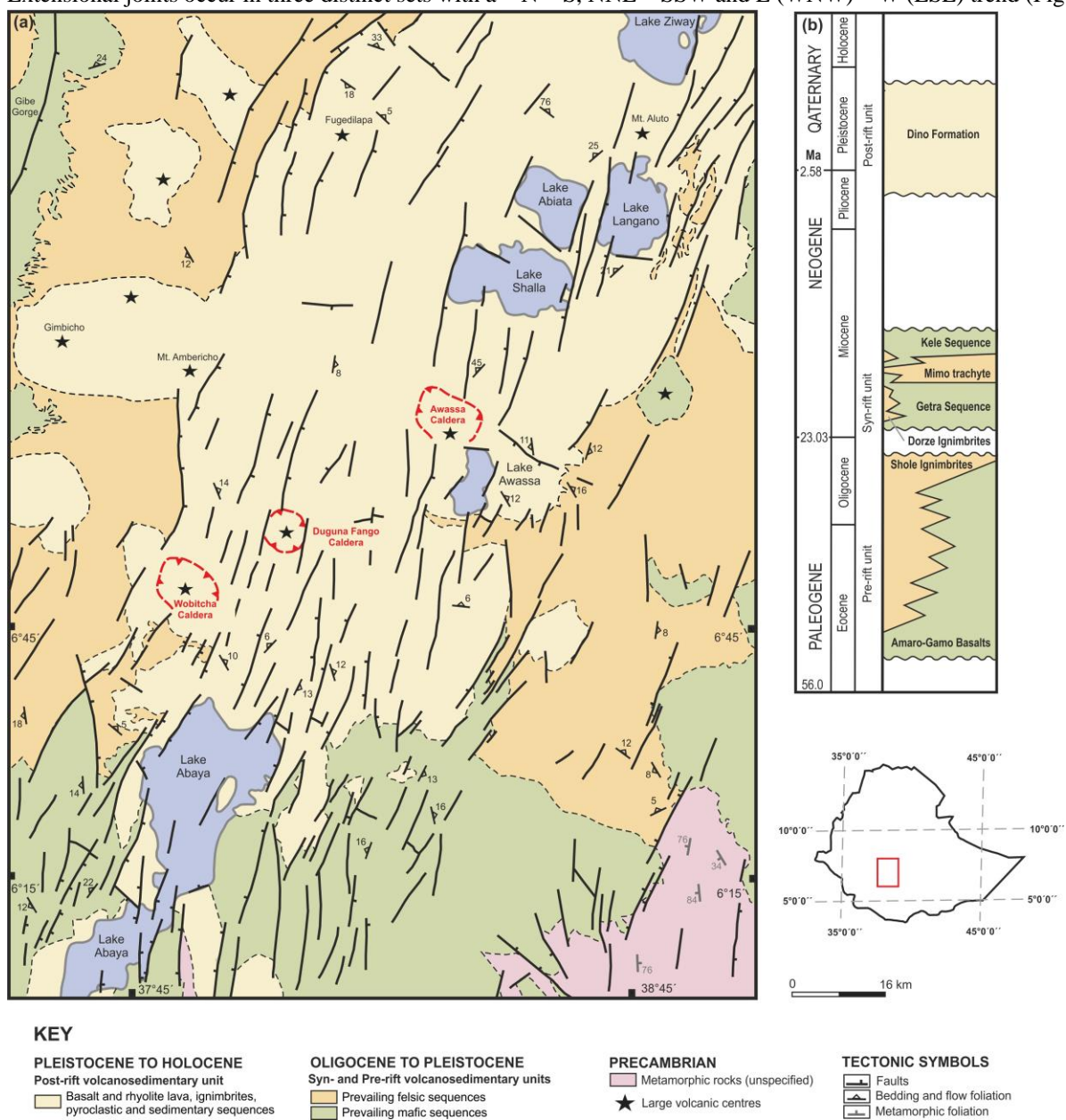


267
 268 *Fig. 3. Morphotectonic analysis of the Dilla and Hossana areas based on morphometry. Linear indices show only*
 269 *lines, which are in accordance with both the visual interpretation of the DEM and the morphometry.*
 270

271 4.2. Tectonics

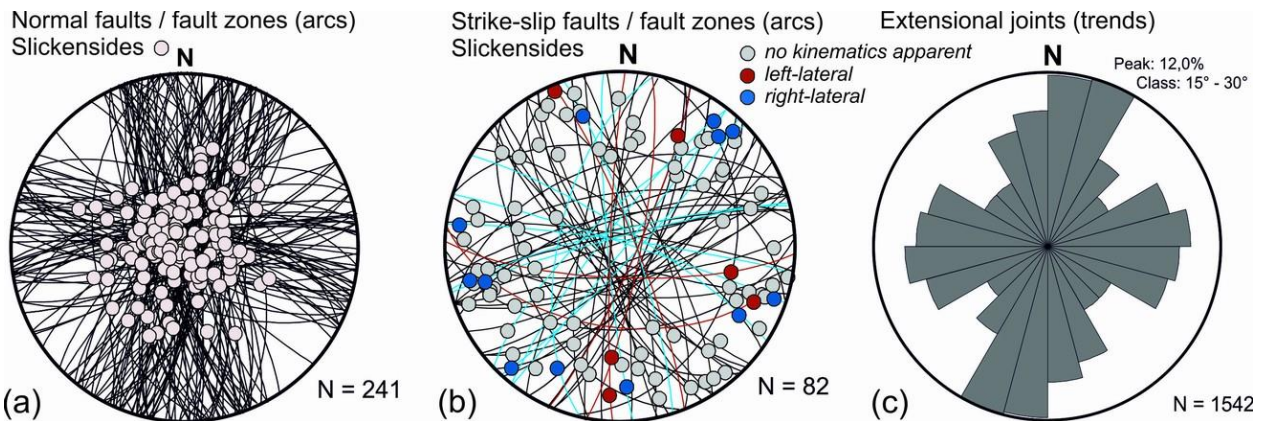
272 The primary fabrics in rift-related volcanic deposits and lava flows are defined by the planar preferred orientation of
 273 rock-forming minerals, micro-vesicles or micro-crystals and elongated mineral grains, lithic fragments or stretched

274 and welded pumice fragments. With the exception of the lateral parts of lava flows or volcanic centres, these planar
 275 fabrics are predominantly flat-lying or dip gently to ~SSW or E. In addition, large amount of fault structures
 276 associated to the ~NNE-SSW trending MERS dip predominantly steeply to ~ESE in the western part of the rift and
 277 to ~WNW along its eastern margin. The main ~NNE-SSW trending faults also form a prominent escarpments and
 278 other morphological features of the MER (Figs. 4 a, 5). These faults are associated with fault lineation (slickensides)
 279 plunging steeply to moderately to ~SE (in the western escarpment) or to ~NW (in the eastern escarpment), both
 280 bearing exclusively normal kinematic indicators (Fig. 6 a, b, c). Two subordinate sets of fault structures appear to be
 281 synchronous with the main ~NNE-SSW faults are mostly perpendicular, WNW(W)-ESE(E) trending normal faults
 282 with predominantly NNW plunging slickensides or steeply ~NNW dipping normal faults (Fig. 5a). Relatively
 283 younger or newly reactivated ~NNW(N)-SSE(S) trending faults which are oblique by ~20-30° to the main fault
 284 system were mapped mainly in the central part of the rift valley (Fig. 2, 5a). In addition, ~NNW – ESE, ~NE-SW
 285 and ~WSW – ENE trending strike-slip faults with a gently prevailing right-lateral kinematic pattern were identified
 286 across the studied area (Fig. 2,5b). In spatial context of large volcanic centres (e.g. Wobitcha, Duguna Fango and
 287 Awassa Caldera; Fig. 2) the caldera-related ring faults were found having a curved asymmetric shape, mostly
 288 parallel to the caldera rim. These faults predominantly dip steeply to moderately inward to the centre of the caldera.
 289 Extensional joints occur in three distinct sets with a ~ N – S, NNE – SSW and E (WNW) – W (ESE) trend (Fig. 5c).



290 **Fig. 4. (a) Simplified geological map of the southern part of the Main Ethiopian Rift (Hossana and Dilla areas); (b)**
 291 **Schematic stratigraphic chart of the Main Ethiopian Rift (Dilla and Hossana areas). Compiled using unpublished**
 292 **geological maps 1:250 000 Geological Survey of Ethiopia.**
 293

294
295



296
297
298
299

Fig. 5. Field structural measurements of faults (equal area projection to lower hemisphere) and extensional joints (rose diagram) from the southern part of the Main Ethiopian Rift (Hossana and Dilla areas).



300
301
302
303
304
305
306
307

Fig. 6. Field photographs (a) Steeply dipping, N – S oriented fault plane with steeply plunging slickensides and normal kinematic indicators (west of Dilla Town, eastern rift escarpment). (b) ESE moderately dipping normal fault, parallel with the main NNE-SSW trending western rift escarpment (Ocholo Village, north of Arba Minch). (c) Steeply dipping, N – S oriented fault plane with steeply plunging slickensides and normal kinematic indicators (Mejo Plateau, ca. 60 km east of the main rift valley). (d) Rockslide and debris flow on normal fault slope north of Arba Minch.

4.3. Areas prone to slope instabilities

308
309
310
311

The principal feature of the MER is the graben bounded by normal faults. The drainage network is largely controlled by tectonic activity and lithological variation. Parts of grabens form endorheic depressions filled by temporal lakes. The area is climatically highly variable; the average amounts of annual rainfall vary from 500 in the Gibe and Omo

312 Gorges to 2,600 mm on the escarpments and the adjacent highlands. The mean annual temperature is about 20°C
313 (Yekoye et al 2012; Habtamu et al 2012; Rapprich and Eshetu 2014; Rapprich et al 2014).
314 Slope failures, erosion, floods and the occurrence of ground fissures are the most common geological hazard
315 investigated in the Hossana and Dilla areas. Landslides, debris flows and rockfalls represent common exogenous
316 hazards distributed mainly on the fault scarps (Fig. 2 and 7 a). The subsidence of the rift floor and consequent uplift
317 of the highland lead to isostatic disequilibrium resulting in intensive head-ward erosion and slope processes. Most of
318 the slope instabilities represent deep seated complex fossil slumps, translational or rotational slides (Fig. 7 b) that
319 host reactivated smaller landslides and debris flows which are triggered by adverse anthropogenic practices (road
320 construction, deforestation, overgrazing) or river undercutting (fig. 7 e, f). The landslides are developed in the
321 succession of competent volcanic rocks – basalts and welded ignimbrites intercalated by highly weathered
322 pyroclastics and horizons of paleosoils following the slip zone of this landslides. The steep slopes the highly
323 decomposed volcanic rocks by columnar jointing are subject of toppling and rockfalls.
324 Rare lateral spread, with typical horst and graben features at the head, encountered in the complex un-welded
325 ignimbrites and unconsolidated pyroclastic deposits with horizons of paleosoils following the slip zone of this
326 landslide (fig. 7 c). Topographic depressions with a higher degree of saturation are often noted to have the long run
327 effect of triggering landslides and debris flow on the slopes below them (fig. 7 d, f). More detailed descriptions of
328 slope instabilities are in section 4.5. and figs. 9 and 11.
329



330
 331 *Fig. 7. Field photographs of various types of geohazards in MER – Hossana and Dilla areas. (a) Toppling and*
 332 *subsequent rock fall of welded ignimbrites in the crown of a deep-seated landslide situated close to a fault scarp in*
 333 *the western highland area (Dilla area; NW of Arba Minch town). (b) Large landslide in Dilla area (5 km SW of*
 334 *Mejo town). (c) Tilted blocks of deep-seated landslide southwest to Awassa. (d) Undrained depression in the deep-*
 335 *seated fossil landslide east of Dilla Town. (e) Tension cracks in the crown of a shallow landslide reactivated by road*
 336 *construction, west of Arba Minch. (f) Recent debris flow accumulation below road construction in the landslide area*
 337 *west of Mejo.*

338
 339 **4.4. Statistical analysis**

340 Statistical analysis was carried out to better understand the influence of various surface processes and conditions
 341 (precipitation, vegetation, slope, land cover) and geological parameters (rock mass strength, proximity of faults,
 342 lineaments) on the formation of landslides and rockfalls. However, anthropogenic factors could not be evaluated
 343 statistically because the relevant data are not available. This section refers to regional mapping 1: 250 000 scale,
 344 where areas prone to geohazards rather than particular geohazards were mapped. The results should be interpreted in
 345 this view.

346

347 **4.4.1. Descriptive statistics**

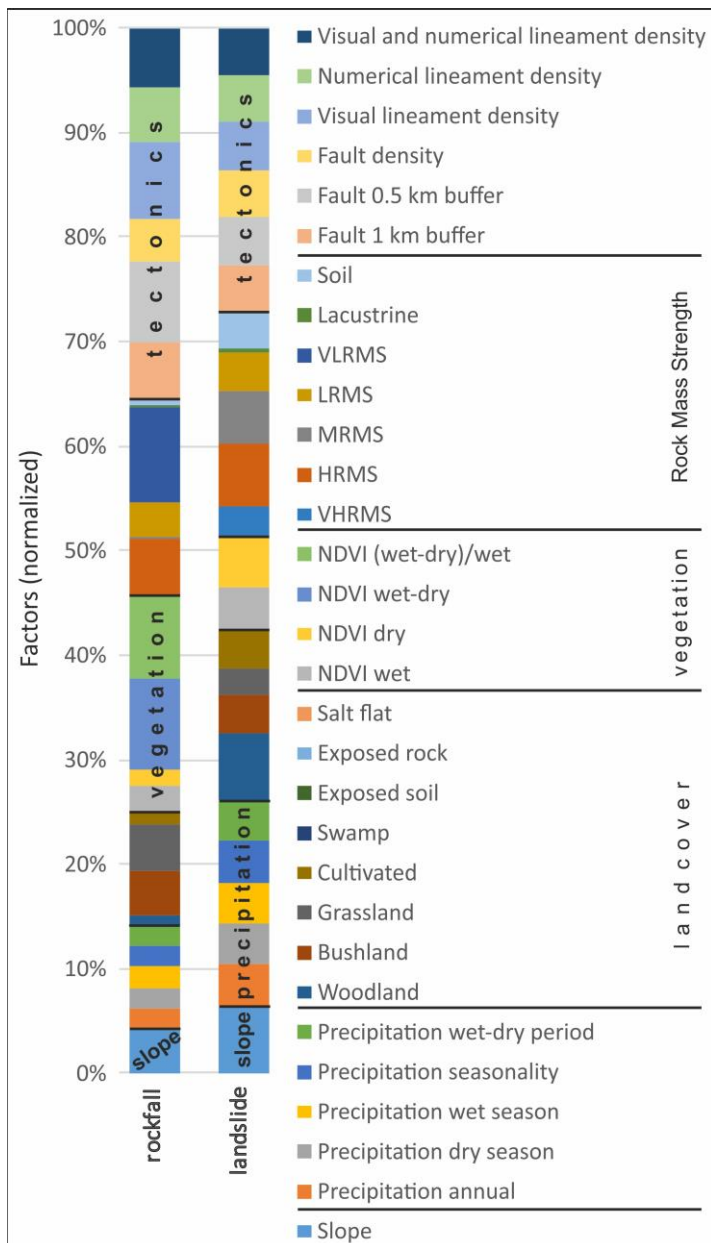
348 For the purposes of descriptive statistics, Rock Mass Strength (RMS) was coded as follows: Very High RMS = 7,
 349 High RMS = 6, Medium RMS = 5, Low RMS = 4, Very Low RMS = 3, Soils = 2, Lacustrine deposits = 1. A
 350 significant correlation between RMS and slope and most precipitation parameters was found (see Table 1). More
 351 wet and seasonal areas occur on steeper slopes formed by stronger (less weathered) rocks. Most of the steep slopes
 352 in the study area are active normal fault escarpments. Another interesting statistically significant correlation is
 353 shown by Slope and most of the precipitation parameters and the vegetation index (NDVI) of the dry period. Steeper
 354 slopes and higher altitudes are attracting clouds and precipitation, while flat lowlands allow clouds to pass by
 355 without precipitation. Significant correlations can also be found within various precipitation parameters, within
 356 selected vegetation parameters and also between these two groups (precipitation and vegetation), which was
 357 supposed. No significant correlation was found between the proximity of faults and lineaments (expressed by faults
 358 and lineaments density) and other parameters. It seems to be an independent variable very suitable for further
 359 geostatistical evaluation. High density of faults and lineaments is in areas where faults and lineaments of different
 360 strikes are crossing, these areas do not necessarily have higher slopes. For other tectonic parameters like faults and
 361 lineament proximity are hardly to calculate conventional correlation, they are evaluated geostatistically in following
 362 sections.
 363

	RMS	Slope	Precipitation					NDVI			Faults and lineaments density
			Annual	Dry period	Wet period	Seasonality	Wet-dry period	Wet period	Dry period	Wet-dry period	
RMS	1.00	0.44	0.49	0.17	0.43	0.58	0.39	0.10	0.07	-0.01	0.13
Slope	0.44	1.00	0.37	0.11	0.25	0.37	0.22	0.16	0.24	-0.12	-0.11
Precipitation annual	0.49	0.37	1.00	0.61	0.47	0.73	0.35	0.28	0.37	-0.16	-0.14
Precipitation dry period	0.17	0.11	0.61	1.00	-0.11	-0.01	-0.27	0.14	0.41	-0.29	-0.18
Precipitation wet period	0.43	0.25	0.47	-0.11	1.00	0.80	0.99	0.15	-0.39	0.44	0.06
Precipitation seasonality	0.58	0.37	0.73	-0.01	0.80	1.00	0.77	0.20	0.06	0.07	0.03
Precipitation wet-dry period	0.39	0.22	0.35	-0.27	0.99	0.77	1.00	0.12	-0.44	0.47	0.09
NDVI wet period	0.10	0.16	0.28	0.14	0.15	0.20	0.12	1.00	0.16	0.46	-0.05
NDVI dry period	0.07	0.24	0.37	0.41	-0.39	0.06	-0.44	0.16	1.00	-0.80	-0.10
NDVI wet-dry period	-0.01	-0.12	-0.16	-0.29	0.44	0.07	0.47	0.46	-0.80	1.00	0.06
Faults and lineaments density	0.13	-0.11	-0.14	-0.18	0.06	0.03	0.09	-0.05	-0.10	0.06	1.00

364
 365 *Table 1. Correlation matrix of the selected factors controlling distribution of geohazards in the MER area. Number*
 366 *of samples 153, critical value for correlation coefficient (R) at the 95 % significance level is 0.195. A statistically*
 367 *significant (95 %) R is in bold.*

368
 369 **4.4.2. Geostatistics**

370 The mean values of various geological, tectonic, climatic, vegetation and land use factors were calculated for each
 371 landslide polygon area. The normalized difference vegetation index (NDVI) is adopted from MODIS images of
 372 2016 while density of lineaments is expressed as *[E+06]. The Kernel Density tool of the Spatial Analyst
 373 Tools/Density (ArcGIS 10.6) was used for evaluating the faults and lineaments density in MER on a scale of 1:250
 374 000 (see Table 2). Proximity to tectonic features is expressed in terms of the percentage area of a particular
 375 geohazard within a particular buffer zone (500 m and 1 km buffer).
 376



377
 378 *Fig. 8. Plot of mean values of particular factors occurring across landslides and rockfalls polygons normalized to*
 379 *the mean value for the whole area. Diagram shows the relative importance of each factor in comparison with the*
 380 *whole set of factors.*

381
 382 Most landslides and rockfalls form on steeper slopes close to faults and in areas with higher lineament density.
 383 Rockfalls are formed on steeper slopes than landslides (Table 2, see also see figs. 2, 9, 11) but slope factor has
 384 higher importance for the formation of landslides (in comparison to other factors, see Fig. 8). Rockfalls typically
 385 occur on areas receiving lower precipitation. Most of them occupy areas with grassland and, to a lesser extent, also
 386 on cultivated land and bush land cover. Higher vegetation seasonality is also found to coincide well with rockfall
 387 occurrences, there is high vegetation difference between dry season (January) and rain season (August, see Table 2).
 388 That is probably because fault escarpment vegetation, which grows in difficult conditions on steep rocky slopes, is
 389 more sensitive to precipitation seasonality. A low, very low and high rock mass strength class probably influence the
 390 occurrence of rockfalls (see Table 2 and Fig. 8) but not medium rock mass strength. Probably because hard rocks are
 391 jointed and then rock falls with big blocks occur, these polygons include also slope deposits, classified as low to
 392 very low RMS. While landslides are formed in areas with higher precipitation and higher precipitation seasonality.
 393 Woodland, bushland, grassland and cultivated areas with higher vegetation density and low vegetation seasonality
 394 are found to have an affinity with landslide occurrences. All range of rock mass strength classes (low, medium and
 395 high) occur in areas of landslides.
 396

geohazard\factor	Slope [degree]	Precipitation			P. seasonality		Vegetation		V. seasonality		Rock Mass Strength						Tectonics		Lineaments density				Landuse							
		annual [mm]	Dec-Jan (Dry) [mm]	Jul-Aug (Wet) [mm]	monthly 1 σ	wet-dry [mm]	NDVI wet (Aug)	NDVI dry (Jan)	NDVI Aug-Jan	(Aug-Jan)/Aug [%]	VHRMS [%]	HRMS [%]	MRMS [%]	LRMS [%]	VL RMS [%]	Lacustrine [%]	Soil [%]	within 1 km buffer	within 0.5 km buffer	faults	visual	numerical	vis and num	woodland [%]	bushland [%]	grassland [%]	cultivated [%]	swamp [%]	exposed soil [%]	water [%]
rockfall	17.2	<i>1041</i>	44	312	54	268	5412	<i>3149</i>	2263	42	0	27	3	40	25	1	3	88	66	155	341	227	227	8	18	48	21	1	0	4
landslide	15.6	1248	51	351	66	300	5296	5510	<i>-214</i>	-4	4	18	38	26	0	1	12	43	24	97	131	111	108	38	9	16	37	0	0	0
whole area	9.0	1172	48	333	61	285	4868	4297	571	12	5	11	28	26	6	11	13	36	19	82	103	95	88	22	9	24	36	1	1	6

Table 2. Mean values for each geohazard polygon area compared to the whole area of Hossana and Dilla. NDVI calculated from Modis images 2016, lineaments density is $\ast[E+06]$. The proximity of tectonics is expressed in the percentage area of the particular geohazard within the buffer. **Bold underline** - highly above average; **bold** - above average; *italics* - below average.

4.5. Case studies – Mejo and Arba Minch areas

Two areas with contrasting lithological, tectonic, climatic and vegetation settings and a similar size and morphology of landslides and rockfalls were selected for a detailed study. The study areas correspond with 1:50 000 mapping (for location of map sheets see Fig. 2).

4.5.1. Mejo Site

Geological and climatic setting

The Mejo study area is located 60 km east of the main rift valley on the upland plateau of the south-eastern flank of the MER. The Gambelto and Genale rivers drain the area southeast to Somalia form a typical morphology with deeply incised N-S trending valleys in the central part and volcanic plateaus along the south-western and eastern margin (Fig. 9). These volcanic plateaus attain an elevation slightly above 2000 m asl at east and around 2,100 m asl at south-west. Neoproterozoic medium-grade metamorphic rocks crop out mainly in the deeper part of the valleys below the altitude of ca 1900 m and the deepest parts reach below 1000 m asl. Thus, the area has a prominent topography with an altitude difference of more than 1000 m; the average slope in the area is more than 14 degrees. The overlying volcanic deposits are of Eocene to Pleistocene age (Verner et al., 2018a; Verner et al., 2018b). The local climate is humid, the annual precipitation is ~1,200 mm to ~1,550 mm (average 1393 mm) and highly seasonal usually with two peaks corresponding to April-May and August-October with more than 125 mm monthly average rainfall, while the rest of the months have a monthly average rainfall of slightly more than 40 mm. The difference between the average wet (July + August) and dry season (December + January) is 310 mm (CDE, 1999). Vegetation cover is dense (NDVI values almost double comparing the Arba Minch area) and moderately seasonal (see Table 3). Due to intense weathering the area is dominated by rocks with low and medium mass strengths. The dominant land cover is woodland and bushland, cultivated areas form up to 25 % of the area.

The area is formed by two units: (i) Metamorphic basement consisting of foliated biotite orthogneiss with minor lenses of amphibolites outcropped in the lower parts of the slope and the bottom of valleys. The orthogneiss is moderately to strongly weathered, the lenses of amphibolites have higher intact strength with a lower degree of weathering. The foliation of metamorphic rocks is often oriented downslope, parallel with the topography of the instable slopes. (ii) The volcanic complex overlying the metamorphic basement is formed by a roughly 500 metre thick succession of basalt and trachybasalt massive lava flows and intercalations of palaeosols, fine basaltic scoria layers and epiclastic deposits up to 2 m thick. The lava flows are moderately to strongly weathered with high fissured permeability, the pyroclastic layers, paleosols and strongly weathered horizons with high content of clay minerals may form semi-horizontal barriers for water movement resulting in higher plasticity and a reduction of permeability (Verner et al., 2018a; Verner et al., 2018b).

Faults

Most of the fault structures were identified in the complex of metamorphic rocks, without evidence of young reactivation. The youngest faults and fault zones belonging to the East African Rift System are rare and have no significant effect on the overall tectonic pattern of the area. These minor faults dip steeply to ~E or ~W, bearing well-developed steeply plunging slickensides and normal kinematics. The minor subordinate set of normal faults have a ~ W (WNW) to E (ESE) trend. The fault displacement is relatively low across the area, reaching a maximum

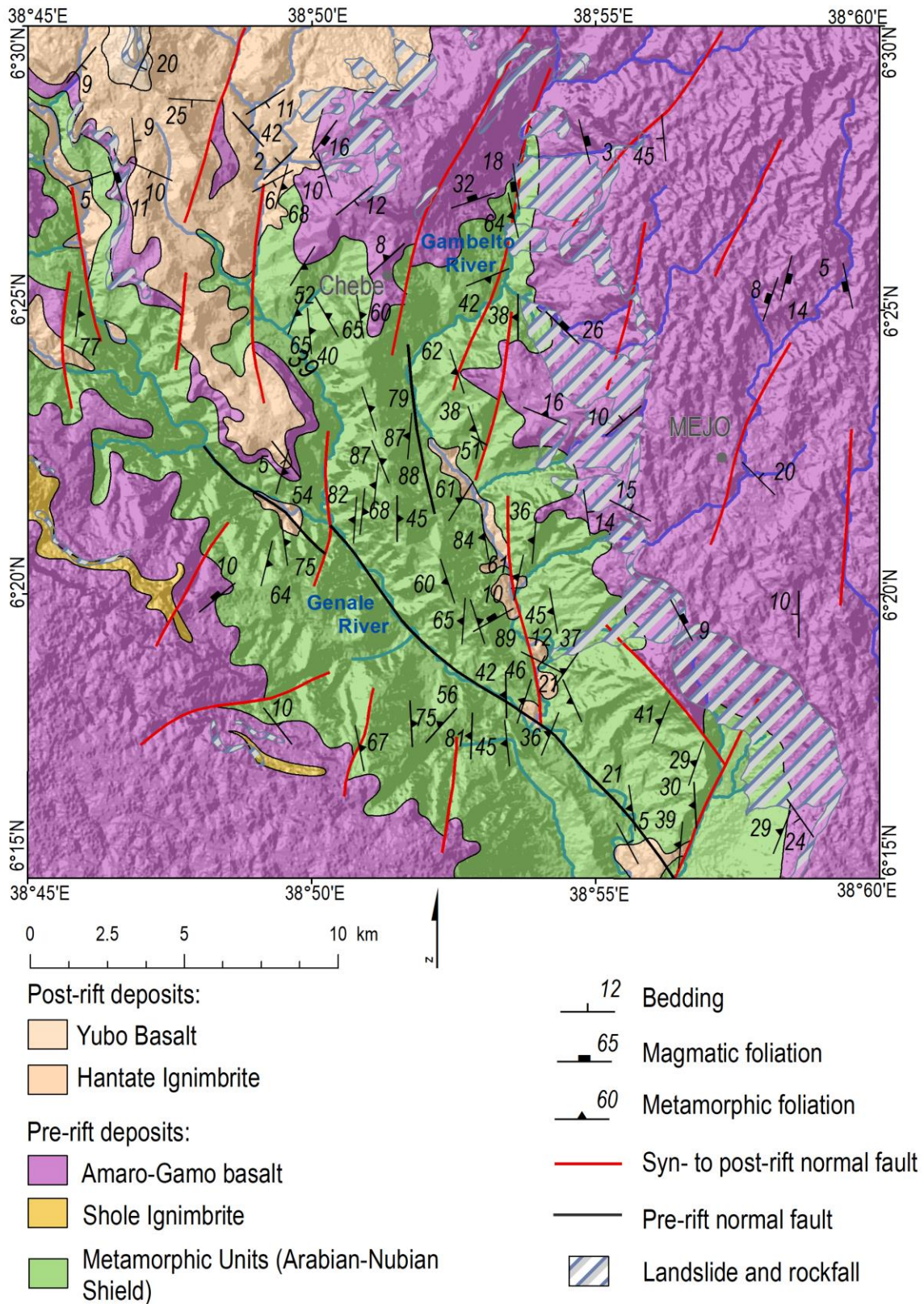
443 of 100 metres in the vertical section (Verner et al., 2018a; Verner et al., 2018b). The prominent morphology, with up
444 to 1000 m deeply incised valleys, is made almost solely by erosion caused by Neogene uplift.

445

446 Landslides and rockfalls

447 A large and deep-seated complex landslide area occurs in the slope of the eastern banks of the Gambelto Valley. The
448 landslide areas vary in length from several hundred metres to 4 kilometres, with a width of up to 2 kilometres (see
449 Fig. 9). The landslide complexes are characterized by amphitheatre (horse-shoe)-shaped edges of the main scarps
450 and reach up to 200 metres high, and 50 to 100 metre high minor scarps. Commonly, tilted blocks, endorheic
451 depressions and a number of springs have also been noted in the landslide zone. Reactivated parts are characterized
452 by small-scale (tens to hundreds of metres) and shallow-seated debris flows, slumps and rock-falls accompanied by
453 the subsidence of surface, cracks or curved tree trunks, which were observed close to the new road construction.
454 Most landslides are fossil and inactive. The preservation of colluvial deposits is limited, while in the depressed
455 domain and the arched accumulation area of the landslide they are covered by boulders and blocks. The morphology
456 of the main and minor scarps is relatively sharp and the accumulation zone is strongly modified by erosional
457 processes with a smooth and undulating topography, an absence of a hummocky landscape and traverse ridges. Most
458 of the reactivated parts are represented by small-scale and shallow-seated failures triggered by the poor design of
459 local road construction.

460



461
 462 *Fig. 9. Geological and tectonic map of the Mejo Site with landslides and rockfalls indicated. For location, see Fig.*
 463 *2.*

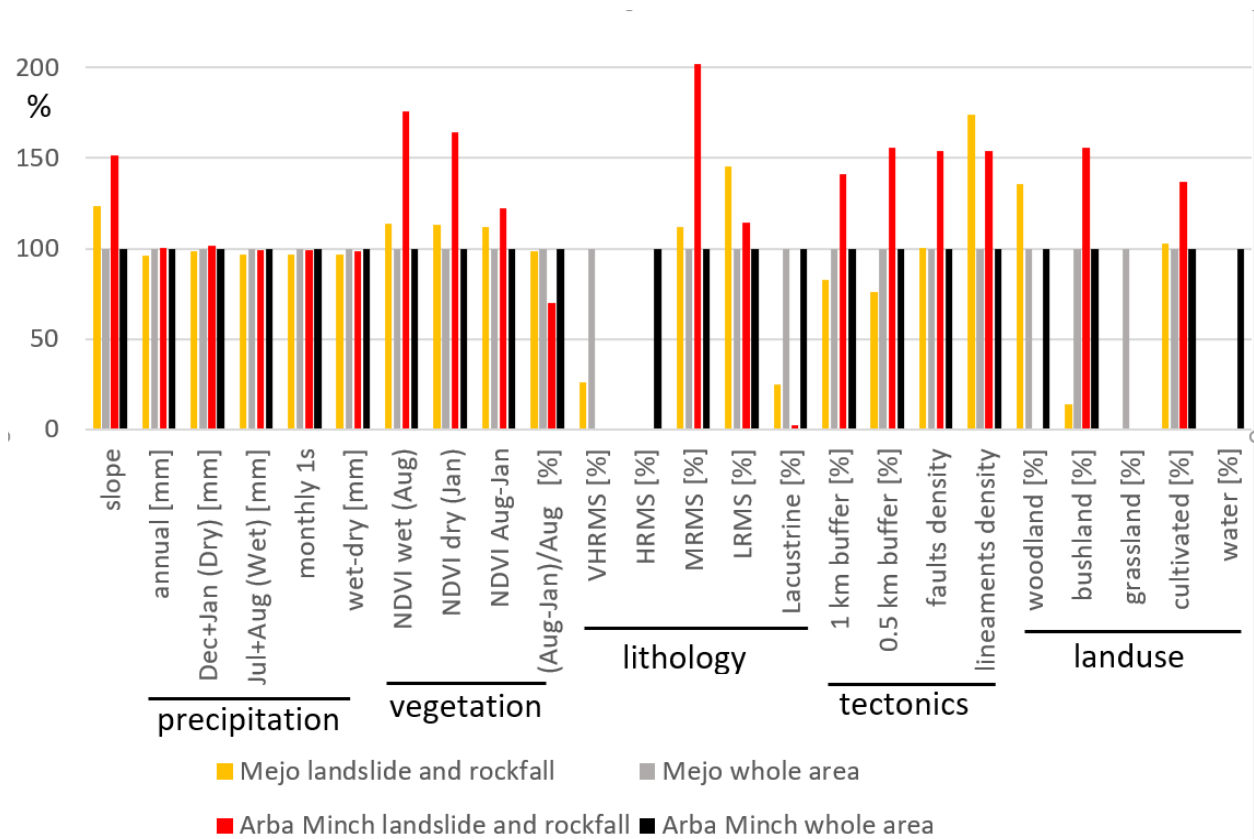
464
 465 Statistical evaluation

466 The mean values of the same factors as for the Hossana and Dilla areas (see section 4.4.2) were also calculated for
 467 each landslide and rockfall polygon area in the case of the Mejo site. The same calculations and symbology as in

468 Table 2 was used for most parameters, but faults and lineaments data were adopted from more detailed studies at a
 469 scale of 1:50 000 (Verner et al., 2018a; Verner et al., 2018b; Verner et al., 2018c; Verner et al., 2018d) and the faults
 470 and lineaments density is calculated by a Line Density tool (ArcGIS 10.6. Spatial Analyst Tools) and expressed as
 471 * $[E+02]$. Here the landslides and debris-flows are situated in areas with much higher slopes, compared to the overall
 472 study area (see Fig. 10 and Table 3). They are also formed in areas with a higher vegetation density and medium and
 473 low RMS. Landslide and debris-flow areas have a much higher density of lineaments. They are also dominantly
 474 vegetated by woodlands, cultivated areas are a minor land cover. Precipitation distribution does not show any
 475 significance, it mean be due to poor spatial resolution of precipitation data. Same applies for Arba Minch area.
 476

geohazard\factor		Slope [degree]	Precipitation		P. seasonality		Vegetation		V. seasonality		Rock Mass Strength				Tectonics			Landuse							
			annual [mm]	Dec-Jan [Dry] [mm]	Jul-Aug [Wet] [mm]	monthly 1g	wet-dry [mm]	NDVI wet (Aug)	NDVI dry (Jan)	NDVI Aug-Jan	(Aug-Jan)/Aug [%]	VHRMS [%]	HRMS [%]	MIRMS [%]	LRMS [%]	Lacustrine [%]	1 km buffer [%]	0.5 km buffer [%]	faults density	lineaments density	woodland [%]	bushland [%]	grassland [%]	cultivated [%]	water [%]
Mejo	landslide and debris-flow	17.6	1335	46	346	75	300	6303	7278	-975	-0.15	2.06		31.7	60.8	5.4	50.9	27	33.8	58	72	3		26	
	whole area	14.2	1393	47	357	78	310	5548	6421	-874	-0.16	7.89		28.3	41.9	22	61.5	36	33.6	34	53	19	3.1	24.8	
Arba	landslide and rockfall	14.9	1070	60	188	45	128	5361	6412	-1051	-0.20			42.7	56.7	0.6	97.1	68	67.0	78		30		70	
Minch	whole area	9.8	1068	59	189	46	130	3051	3909	-858	-0.28		3.01	21.2	49.5	26	68.8	44	43.6	51	1.14	19.2		51.2	28.4

477
 478 Table 3. Mean values for each geohazard polygon area compared to the overall area of Mejo and Arba Minch
 479 respectively.
 480



481
 482 Fig. 10. Plot of mean values of particular factors occurring across merged polygons of landslides and rockfalls
 483 normalized to the mean value for the overall area. Mejo and Arba Minch sites evaluated separately.
 484

485 4.5.2. Arba Minch Site

486 Geological and climatic setting

487 The Arba Minch study area is located directly in the main rift valley on the western normal fault escarpment. The
 488 total displacement of the syn- and post-rift normal faults is more than 1500 metres. The average slope in the area is
 489 less than 10 degrees because a large part of the area is covered by Abaya Lake (see Fig. 11). The area is less humid,
 490 compared to Mejo, with an average annual precipitation of 1068 mm and precipitation is moderately seasonal, the
 491

492 difference between the wet and dry season is 130 mm. But significant variations in precipitation have been recorded
493 in apical parts of mountain ridges, such as Chench, attaining, on average, an altitude of 2,700 m asl with 1,390 mm
494 of rainfall, whereas in the low-lying plains with an average elevation of about 1,200 m asl around the city of Arba
495 Minch the precipitation fluctuates around 780 mm (CDE, 1999). Vegetation cover is moderate (NDVI values almost
496 half of Arba Minch area) and moderately seasonal (see Table 3). Rocks with low and medium mass strengths and
497 lacustrine deposits dominate the area. The dominant land cover type is cultivated areas (form up to 51 %), bushland
498 and water surface are also abundant types. The area is formed by lower Eocene to Pleistocene volcanic and
499 volcanoclastic rocks, which are a product of episodic eruptions. They mostly have a bimodal composition with
500 alternating basic volcanic rocks and acidic pyroclastic rock intercalations (Verner et al., 2018 c; Verner et al.,
501 2018d).

502

503 Faults

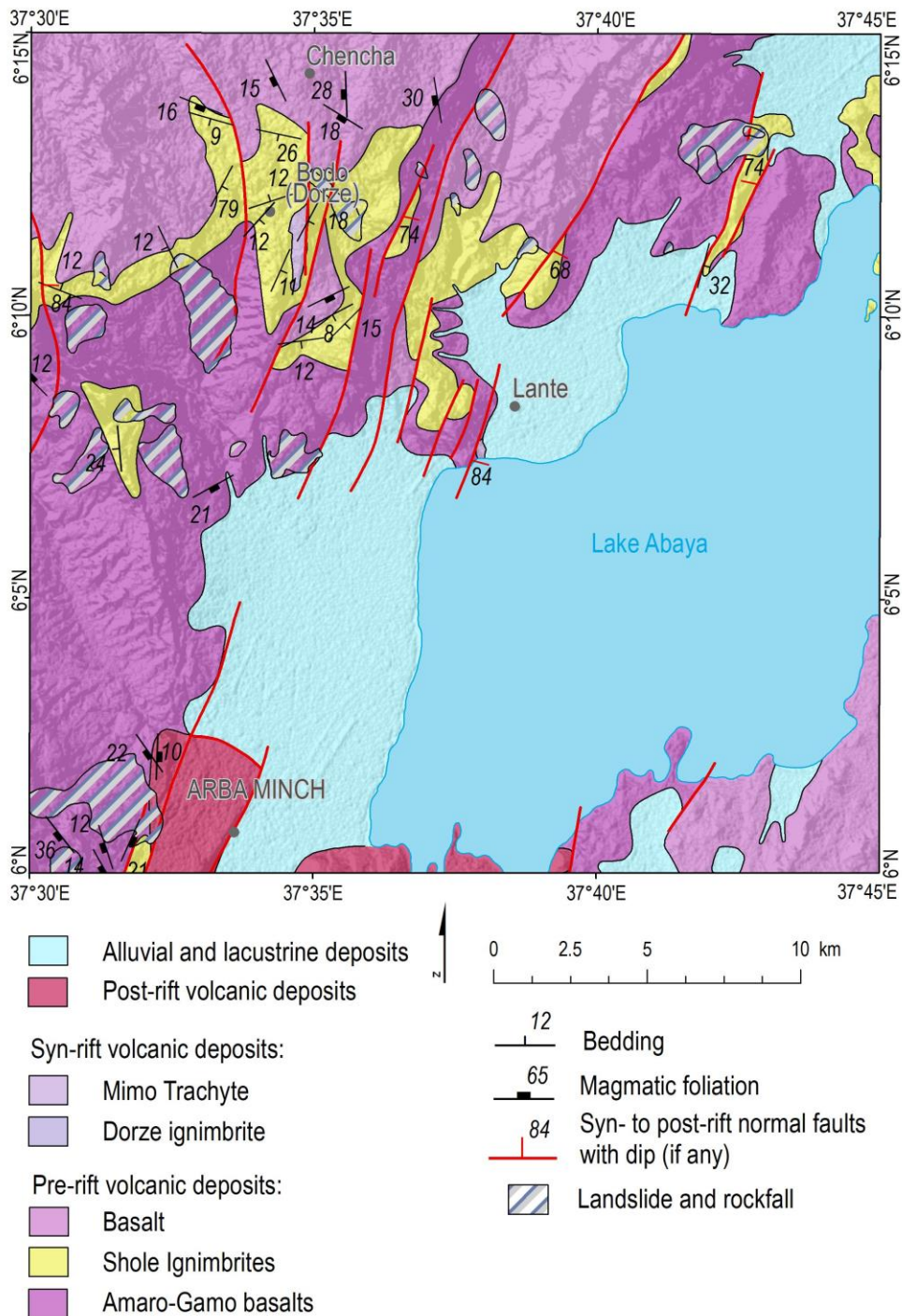
504 The prevailing faults are mostly parallel to the axis of the MER forming the area's prominent morphological
505 features. These major normal faults dip steeply to ESE or SE, trending NNE–SSE. Moreover, subordinate normal
506 faults were identified, predominantly steeply inclined faults trending WNW–ESE, which are perpendicular to the
507 prevailing rift-parallel normal faults. Fault displacement is relatively high across the area, reaching a minimum of
508 1,000 metres forming prominent morphology with an altitude difference of up to 1,500 m between the plateau and
509 graben floor.

510

511 Landslides and rockfalls

512 The slope failures are located in the western steep fault scarps separating the bottom of the rift valley with Abaya
513 Lake representing a local erosional base at an elevation of 1,200 m asl and the western highland with an undulating
514 landscape at an elevation of between 2,000 and 2,400 m asl. The scarps are often modified by deep-seated slope
515 failures. The lower parts of the slopes form moderately weathered basalts and trachybasalt with minor pyroclastic
516 fall layers of volcanic ash reaching up to 2 m in thickness and a reddish paleosol up to 30 cm thick. The ridges and
517 upper parts are formed of welded ignimbrites with minor rhyolitic ash fall deposits and paleosol horizons. Volcanic
518 rocks are variably affected by intense fracturing, jointing and mega tectonic fault systems. Basalts and trachybasalts
519 are with a higher degree of weathering, while the welded ignimbrites with common columnar jointing are more
520 resistant. The volcanic units have fissured permeability. Mainly the ignimbrites represent rocks with high
521 permeability, on the other hand the highly weathered basalt, the intercalation of fine grained pyroclastics and
522 paleosol horizons could form hydrogeological horizontal barriers because of the high content of clay minerals. Most
523 of the landslides are represented by deep-seated complex slope deformations including toppling, rock-fall, rockslide,
524 rotational landslides and debris flows. These slope failures appear to be currently stable; the morphology is modified
525 by subsequent exogenous processes as in the Mejo area. Only several small-scale active landslides triggered by river
526 erosion and human intervention were observed.

527



528
529 *Fig. 11. Geological and tectonic map of Arba Minch Site with landslides and rockfalls indicated. For location, see*
530 *Fig. 2.*

531
532 **Statistical evaluation**
533 The mean values of the same factors as for the Mejo site were also calculated for each landslide and rockfall
534 polygon area at the Arba Minch site. Here the landslides and rockfalls are situated in areas with much higher slopes,
535 compared to the overall study area (see Fig. 10 and Table 3), there is a much higher density of faults and lineaments
536 close to faults. They are also formed in areas with much higher vegetation density and medium and low RMS.
537 Landslide and rockfall areas are also dominantly covered by cultivated areas with woodlands taking a minor role.
538

539 **5. Discussion**

540 **5.1. Main Ethiopian Rift (Hossana and Dilla area)**

541 The progressive changes of the paleo-stress regime during the active continental extension and faulting in the MERS
542 (e.g., Corti et al. 2018; Zwaan and Schreurs, 2020) increase the tectonic anisotropy of rocks, slope instabilities along
543 major and subordinate fault escarpments which have a pronounced effect on the genesis and formation of landslides.
544 Several tectonic models explain the kinematics and paleostress conditions of the regional extension / transtension
545 from the beginning of the rifting (ca 12 Ma) to the present (for the review see Zwaan and Schreurs, 2020). Some
546 models suppose continuous a NW – SE oriented extension (e.g., Chorowicz, 2005) in the early phase which later
547 changed to its current E-W direction (Bonini et al., 2005; Wolfenden et al., 2004). Alternatively, other models also
548 assume a permanent E – W to ESE – WNW oriented extension (e.g., Agostini et al., 2009; Erbello and Kidane,
549 2018).

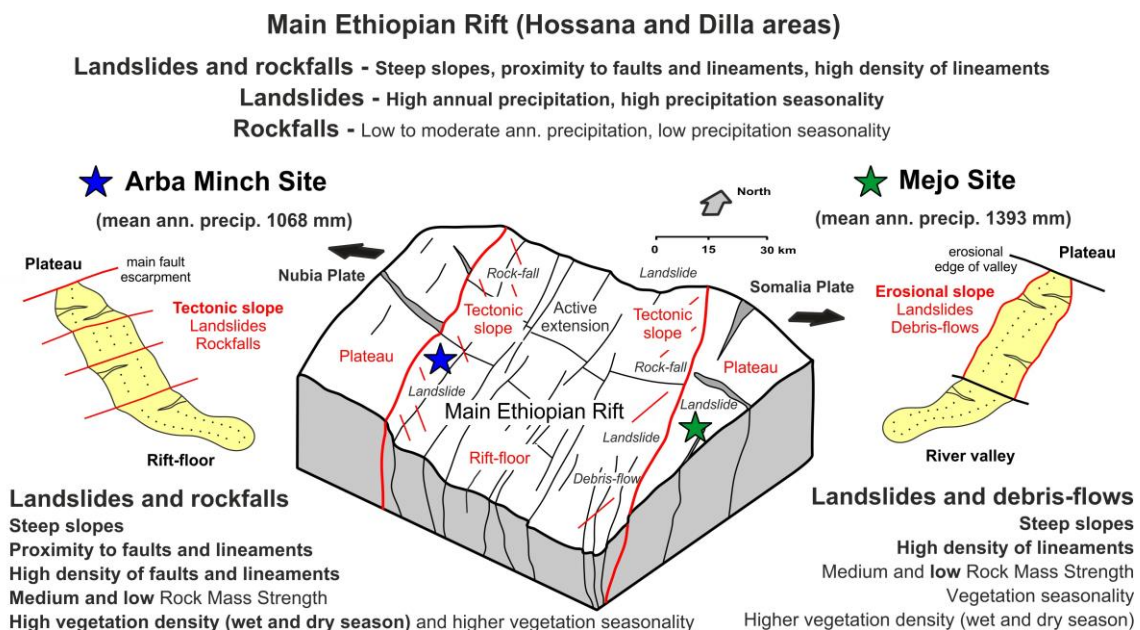
550 Proximity to faults and lineaments have strong influence on the occurrence of rock falls and landslides in
551 tectonically active areas worldwide (e.g., Chang et al, 2018; Kumar et al., 2019 and references therein). In the MER,
552 both rockfalls and landslides typically occur on areas with steep slope, close to faults and with higher density of
553 faults and lineaments. The latter parameter also reflects faults and fracture zone intersections and, according to
554 geostatistic evaluation (Table 2), is more important for the formation of rockfalls than landslides. Rockfalls also
555 show a much higher affinity to the proximity of faults. Most of them are normal faults associated with fissures
556 opening during weathering, which initiates later rockfalls.

557 Rockfalls occur in areas with lower precipitation, while for landslides high precipitation and high precipitation
558 seasonality is typical. It correlates well with high vegetation density and low vegetation seasonality, which are found
559 to have strong affinity with landslide occurrences. Thus, precipitation does not seem to be an important factor for
560 rockfall formation but is important for landslides. Its probably because rockfalls are mapped on fault escarpments
561 close to rift valley, which is more dry, but they are initiated upslope at the edge of plateau where precipitation is
562 higher.

563 Rockfalls and landslides occur on areas with bushland, grassland and cultivated landcover. It leaves deforestation as
564 one of the possible triggering factors. They also occur in areas with a wide range of rock mass strength classes (very
565 low, low, medium and high) so lithology and intensity of weathering do not seem to be an important triggering
566 factor.

567 In the large area of the MER the vast majority of slope instabilities is located on active normal fault escarpments
568 (Fig. 12). This is a major natural triggering factor for rockfalls. While for landslides there is also the important
569 influence of higher precipitation, precipitation seasonality and vegetation density and vegetation seasonality.

570



571 Fig. 12. Sketch diagram summarising the main factors controlling the formation and distribution of particular slope
572 failures in the MER and in the Arba Minch and Mejo study sites.
573
574

5.2. Arba Minch case study

Slope instabilities, mostly landslides and rockfalls, here are situated in areas with much steeper slopes, a much higher density of faults and lineaments and close to major faults. The majority of the large-scale slope instabilities of this area is strongly associated with active tectonic morphological features characterized by straight fault scarps with triangular facets, large downthrown blocks, parallel sets of erosional valleys and asymmetrical ridges with SSW-NNE trending. These features are associated with active normal faults having large displacements (total vertical displacement of the western rift escarpment is more than 1500 m). Slope instabilities are also formed in areas with a much higher vegetation density and medium and low RMS. Volcanic rocks are variably affected by intense fracturing along faults, these zones are often altered, which lowers the slope stability of the rock environment. Alteration is also enhanced by more intense water-rock interactions – most springs are located on fault zones (Arba Minch means “Forty Springs”). Precipitation was not confirmed as an important factor. The Arba Minch area is seismically active, according to the catalogue of earthquakes of the United States Geological Survey (USGS) several earthquakes have been documented around Abaya Lake since 1973 with magnitudes between 4 and 6 (USGS, Earthquake Hazards Program, 2017). This active tectonic is also documented by young faults affecting Quaternary volcanic rocks and sediments outcropped around the town of Arba Minch (Verner et al., 2018 c, d).

5.3. Mejo case study

Landslides and debris-flows here are situated in areas with steep slopes. The geomorphology of the area is almost unaffected by local faults parallel with rift valley; evidence of young faulting as displacement of the Pleistocene and Holocene rocks, straight fault scarps with triangular facets, has not been observed. The steep slopes are formed and strongly modified by intensive head-ward erosion. The incision of the valley as a result of a lowered erosional level and highland uplift could be the driving factor for the slope instability in the case of the Mejo area. Geomorphic proxies and the thickness of flood basalts suggest that the more tectonically active south-eastern escarpment of the CMER and SMER (where the Mejo site is situated) are experiencing a relatively higher rate of tectonic uplift compared to the south-eastern escarpment of the northern MER and the Afar Depression (Xue et al., 2018; Sembroni et al., 2016). This can also be noted from the Eocene-Oligomiocene basalts base (35 – 26 My) occurring in Arba Minch at an elevation of around 1050 m asl compared to their occurrence at a much higher elevation in Mejo, at around 1900 m asl (Verner et al., 2018a; Verner et al., 2018b; Verner et al., 2018c; Verner et al., 2018d). Another factor causing the decrease of slope stability could be local lithological properties (dominance of medium and low RMS characteristic for slope instabilities in the area): (i) frequent intercalations of palaeosols with a high content of clay minerals and low permeability, (ii) a strongly weathered metamorphic basement with foliation often concordant with the landscape forming a very weak lithological environment, which is favourable for slope processes. No young volcanic features and products have been observed; the probability of earthquakes related to volcanic eruptions is very low in the Mejo area, where the nearest earthquakes were recorded 60 km NW of the study area.

5.4. Comparison of Arba Minch and Mejo sites

Landslides at both sites are similar from the geomorphological point of view, i.e., old, stabilized, smoothed by erosion. Estimated age of landslides is Plio-Pleistocene, maybe even older, and uplift dates minimum last several Ma, i.e., approximately the same interval plus Holocene, so in both cases we are dealing with long term evolution. Young reactivations are very localized and mostly due to human activity. Both study areas have seasonal humid climates with a prominent summer (mid June – mid September) rain season, but the Mejo study area, which is situated 90 km east of Arba Minch, 60 km out of the main rift valley on the uplifting plateau, is more humid. In the Mejo area the mean annual rainfall is 30 % higher (1393 mm) compared to Arba Minch (1068 mm), most of the precipitation difference falls in the rainy season, while during the dry months the precipitation at both localities is comparable (Table 3).

Steep slopes associated with active faulting and hydrogeological conditions favouring rock alterations along these zones are probably the main factors triggering the formation of slope instabilities in Arba Minch. In addition to these factors, seismic events could also be speculated as one of the triggering factors.

The combination of a deeply weathered Proterozoic basement and steep slopes formed by intense head-ward erosional processes due to relatively rapid uplift could represent the main factors for creating favourable conditions for landslide evolution in Mejo (Fig. 12). More intense precipitation may also contribute to slope instability.

629 **6. Conclusions**

630 Active continental rifting has a distinct effect on the formation of landslides. The formation, superposition, and
631 polyphase reactivation of fault structures in the changing regional stress-field increase the tectonic anisotropy of
632 rocks and increase the risk of slope instabilities forming. The new structural data from the CMER and SMER
633 support a model of progressive change in the orientation of the regional extension from NW – SE to the recent
634 E(ENE) – W(WSW) direction driven by the African and Somalian plates moving apart with the presumable
635 contribution of the NNE(NE) – SSW(SE) extension controlled by the Arabic Plate.
636 An evaluation at the regional scale of the central and southern MER demonstrates that slope instabilities, mainly
637 landslides and rockfalls, occur on steep slopes, which were almost exclusively formed on active normal fault
638 escarpments. Landslides are also importantly influenced by higher annual precipitation, higher precipitation
639 seasonality and vegetation density and seasonality, while rockfalls have an affinity to vegetation seasonality only.
640 Landslides occur on slopes in higher altitudes with higher precipitation and vegetation density, but large parts of
641 study area are on rift floor, which is more dry, scarcely vegetated, very flat and without landslides, while on
642 rockfalls occupying very steep rocky and blocky fault escarpments dense vegetation can not develop. Deforestation
643 is also important predisposition, because rockfalls and landslides typically occur on areas with bushland, grassland
644 and cultivated landcover.
645 Different geological, geomorphological, and climatic conditions can lead to formation of similar types of slope
646 instabilities. A detailed study on active rift escarpment in the Arba Minch area revealed similar affinities as in the
647 regional study of MER. Slope instabilities here are closely associated with steep, mostly faulted, slopes and a higher
648 density of vegetation. Active faulting forming steep slopes is the main predisposition for landslide formation here,
649 and the main triggers could be seismicity and seasonal precipitation.
650 While the detailed study situated in the Mejo area on the uplifting Ethiopian Plateau 60 km east of the rift valley
651 show that the occurrence of slope instabilities is strongly influenced by steep erosional slopes and deeply weathered
652 Proterozoic metamorphic basement. Landslides here are often formed in areas densely fractured and with foliation
653 concordant with topography. Regional uplift accompanied by rapid head-ward erosion forming steep slopes together
654 with unfavourable lithological conditions is the main predisposition for landslide formation, the main triggers can be
655 intense precipitation and higher precipitation seasonality. Triggers for young landslides are also very probably
656 human activity and erosion, but for thorough evaluation relevant data are missing, only occasional observations
657 support this conclusion.

658
659

660 *Data availability.* Data are available upon request with the corresponding author.

661

662 *Author contribution.* Karel Martínek prepared the manuscript with contributions from all co-authors, he performed
663 morphotectonic study, remote sensing data processing and analysis, statistic and geostatistical analysis and part of
664 the field geological mapping. Kryštof Verner was responsible for structural analysis and part of the field geological
665 mapping. Tomáš Hroch performed the geohazard mapping and analysis. Leta A. Megerssa contributed with climatic
666 and engineering geology data and did part of the field geohazard mapping. Veronika Kopačková performed
667 morphometric analysis. David Buriánek carried out part of the field geological mapping and provided information
668 on rock lithologies. Ameha Muluneh contributed to structural analysis, Radka Kalinová helped with manuscript
669 preparation and Miheret Yakob with Muluken Kassa did important parts of field mapping.

670

671 *Competing interests.* The authors declare that they have no conflict of interest.

672

673 *Acknowledgements.* The research was funded by the Czech Development Agency in the framework of development
674 project No. 281226/2018-ČRA “Implementation of a Methodical Approach in Geological Sciences to Enhance the
675 Quality of Doctoral Studies at the Addis Ababa University (Ethiopia)” (to K. Verner) and project No. 280614/2019-
676 ČRA “Ensuring Sustainable Land Management in Selected Areas of Ethiopia on the Basis of Geoscientific
677 Mapping” (to K. Verner). We thank our many colleagues from the Geological Survey of Ethiopia and Addis Ababa
678 University (School of Earth Sciences) for their help in the acquisition, processing and interpretation of the data,
679 especially to Aberash Mosisa and Wubayehu Dessalegn Sallile. Many thanks to Richard Withers for the English
680 proof reading. Manuscript was enhanced by valuable comments of the editor Prof. Filippo Catani and two
681 anonymous referees.

682

683 **References**

- 684
- 685 Abate, M., Nyssen, J., Steenhuis, T. S., Moges, M. M., Tilahun, S. A., Enku, T., and Adgo, E.: Morphological
686 changes of Gumara River channel over 50 years, upper Blue Nile basin, Ethiopia, *Journal of Hydrology*,
687 525, 152-164, <https://doi.org/10.1016/j.jhydrol.2015.03.044>, 2015.
- 688 Abebe, T., Manetti, P., Bonini, M., Corti, G., Innocenti, F., Mazzarini, F., and Pecskey, Z.: Geological map (scale
689 1:200 000) of the northern main Ethiopian rift and its implication for the volcano-tectonic evolution of the
690 rift, Geological Society of America, Boulder, Colorado, Maps and Charts series, MCH094, 2005.
- 691 Abebe, B., Dramis, F., Fubelli, G., Umer, M., and Asrat, A.: Landslides in the Ethiopian highlands and the Rift
692 margins, *Journal of African Earth Sciences*, 56, 131-138, <https://doi.org/10.1016/j.jafrearsci.2009.06.006>,
693 2010.
- 694 Acocella, V.: Coupling volcanism and tectonics along divergent plate boundaries: Collapsed rifts from central Afar,
695 Ethiopia, *Geological Society of America Bulletin*, 122, 1717–1728, <https://doi.org/10.1130/B30105.1>,
696 2010.
- 697 Agostini, A., Corti, G., Zeoli, A., and Mulugeta, G.: Evolution, pattern, and partitioning of deformation during
698 oblique continental rifting: Inferences from lithospheric-scale centrifuge models, *Geochemistry*,
699 *Geophysics*, *Geosystems*, 10, 1-11, <https://doi.org/10.1029/2009GC002676>, 2009.
- 700 Agostini, A., Bonini, M., Corti, G., Sani, F., and Manetti, P.: Distribution of Quaternary deformation in the central
701 Main Ethiopian Rift, East Africa, *Tectonics*, 30, <https://doi.org/10.1029/2010TC002833>, 2011.
- 702 Altin, T. B. and Altin, B. N.: Development and morphometry of drainage network in volcanic terrain, Central
703 Anatolia, Turkey, *Geomorphology*, 125, 485–503, <https://doi.org/10.1016/j.geomorph.2010.09.023>, 2011.
- 704 Asfaw, L. M.: Development of earthquake-induced fissures in the Main Ethiopian Rift, *Nature*, 297, 393-395,
705 <https://doi.org/10.1038/297393a0>, 1982.
- 706 Asfaw, L. M.: Seismic risk at a site in the East African rift system, *Tectonophysics*, 209, 301-309,
707 [https://doi.org/10.1016/0040-1951\(92\)90038-8](https://doi.org/10.1016/0040-1951(92)90038-8), 1992.
- 708 Asfaw, L. M.: Environmental hazard from fissures in the Main Ethiopian Rift, *Journal of African Earth Sciences*, 27,
709 481-490, [https://doi.org/10.1016/S0899-5362\(98\)00074-8](https://doi.org/10.1016/S0899-5362(98)00074-8), 1998.
- 710 Asfaw, L. M.: Integrated approach to the study of geohazards with application in southern Afar, *Journal of African*
711 *Earth Sciences*, 48, 237–244, <https://doi.org/10.1016/j.jafrearsci.2006.08.006>, 2007.
- 712 Ayalew, L. and Yamagishi, H.: Slope failures in the Blue Nile basin, as seen from landscape evolution perspective,
713 *Geomorphology*, 57, 95–116, [https://doi.org/10.1016/S0169-555X\(03\)00085-0](https://doi.org/10.1016/S0169-555X(03)00085-0), 2004.
- 714 Ayalew, L.: Analysing the effects of historical and recent floods on channel pattern and the environment in the
715 Lower Omo basin of Ethiopia using satellite images and GIS. *Environmental geology* 58, 8, 1713-1726,
716 2009.
- 717 Ayalew, L., Yamagishi, H.: Slope failures in the Blue Nile basin, as seen from landscape evolution perspective.
718 *Geomorphology* 57, 95-116, 2004.
- 719 Ayalew, L., Yamagishi, H., and Reik, G.: Ground cracks in Ethiopian Rift Valley: facts and uncertainties,
720 *Engineering Geology*, 75, 309–324, <https://doi.org/10.1016/j.enggeo.2004.06.018>, 2004.
- 721 Ayalew, L., Möller, D.P. and Reik, G.: Using artificial neural networks (ANN) for real time flood forecasting, the
722 Omo River case in southern Ethiopia. In *Proceedings of the 2007 Summer Computer Simulation*
723 *Conference* (p. 19). Society for Computer Simulation International. 2007.
- 724 Ayele, A.: Probabilistic seismic hazard analysis (PSHA) for Ethiopia and the neighboring region, *Journal of African*
725 *Earth Sciences*, 134, 257–264, <https://doi.org/10.1016/j.jafrearsci.2017.06.016>, 2017
- 726 Ayele, A., Jacques, E., Kassim, M., Kidane, T., Omar, A., Tait, S., Necessian, A., de Chabaliere, J. B., and King, G.:
727 The volcano–seismic crisis in Afar, Ethiopia, starting September 2005, *Earth and Planetary Science Letters*,
728 255, 177–187, <https://doi.org/10.1016/j.epsl.2006.12.014>, 2007.
- 729 Ayele, A., Keir, D., Ebinger, C., Wright, T. J., Stuart, G. W., Buck, W. R., Jacques, E., Ogubazghi, G., and Sholan,
730 J.: September 2005 mega-dike emplacement in the Manda-Harraro nascent oceanic rift (Afar Depression),
731 *Geophysical Research Letters*, 36, <https://doi.org/10.1029/2009GL039605>, 2009.
- 732 Ayenew, T. and Barbieri, G.: Inventory of landslides and susceptibility mapping in the Dessie area, northern
733 Ethiopia, *Engineering Geology*, 77, 1–15, <https://doi.org/10.1016/j.enggeo.2004.07.002>, 2005.
- 734 Beyene, A. and Abdelsalam, M.G.: Tectonics of the Afar Depression: A review and synthesis. *Journal of African*
735 *Earth Sciences* 41, 1-2, 41-59, 2005.

- 736 Billi, P.: Geomorphological landscapes of Ethiopia, In *Landscapes and Landforms of Ethiopia*, Springer, Dordrecht,
737 3-32 pp., https://doi.org/10.1007/978-94-017-8026-1_1, 2015.
- 738 Billi, P. and Dramis, F.: Geomorphological investigation on gully erosion in the Rift Valley and the northern
739 highlands of Ethiopia, *Catena*, 50, 353–368, [https://doi.org/10.1016/S0341-8162\(02\)00131-5](https://doi.org/10.1016/S0341-8162(02)00131-5), 2003.
- 740 Boccaletti, M., Mazzuoli, R., Bonini, M., Trua, T., Abebe, B.: Plio-Quaternary volcanotectonic activity in the
741 northern sector of the Main Ethiopian Rift: relationships with oblique rifting. *Journal of African Earth*
742 *Sciences* 29, 679-698, 2009.
- 743 Bolongaro-Crevenna, A., Torres-Rodríguez, V., Sorani, V., Frame, D., and Ortiz, M. A.: Geomorphometric analysis
744 for characterizing landforms in Morelos State, Mexico, *Geomorphology*, 67, 407–422,
745 <https://doi.org/10.1016/j.geomorph.2004.11.007>, 2005.
- 746 Bonini, M., Souriot, T., Boccaletti, M., Brun, J.P.: Successive orthogonal and oblique extension episodes in a rift
747 zone: Laboratory experiments with application to the Ethiopian Rift. *Tectonics* 16, 347-362, 1997.
- 748 Bonini, M., Corti, G., Innocenti, F., Manetti, P., Mazzarini, F., Abebe, T., and Pecskey, Z.: Evolution of the Main
749 Ethiopian Rift in the frame of Afar and Kenya rifts propagation, *Tectonics*, 24, 1–24,
750 <https://doi.org/10.1029/2004TC001680>, 2005.
- 751 British Standard BS5930: Code of Practice for Site Investigations, British Standards Institution (BSI), London, 147
752 pp., <https://doi.org/10.3404/00056552>, 1981.
- 753 Burianek, D., Hroch, T., Verner, K., Megerssa, L., Martinek, K., Yakob, M., Haregot, A., Janderkova, J., Sima, J.,
754 Krystofova, E., Valenta, J., Tadesse, E., Mosisa, A., Dalke, G., Legesse, F., Assefa, G., Pecskey, Z.,
755 Hejtmankova, P., and Krejci, Z.: Explanatory notes to thematic geoscientific maps of Ethiopia at a scale of
756 1: 50,000, Map Sheet 0638-C2 Dila. Czech Geological Survey, Prague, 103 pp, 2018.
- 757 Centre for Development and Environment: Ethio GIS CD-ROM Database file system, University of Bern,
758 Switzerland, 1999
- 759 Chang, K.-J., Chan, Y.-Ch., Chen, R.-F., and Hsieh, Y.-Ch.: Geomorphological evolution of landslides near an
760 active normal fault in northern Taiwan, as revealed by lidar and unmanned aircraft system data, *Nat.*
761 *Hazards Earth Syst. Sci.*, 18, 709–727, <https://doi.org/10.5194/nhess-18-709-2018>, 2018.
- 762 Chorowicz, J.: The east African rift system, *Journal of African Earth Sciences*, 43, 379–410,
763 <https://doi.org/10.1016/j.jafrearsci.2005.07.019>, 2005.
- 764 Corti, G.: Continental rift evolution: From rift initiation to incipient break-up in the Main Ethiopian Rift, East
765 Africa, *Earth-Science Reviews*, 96, 1–53, <https://doi.org/10.1016/j.earscirev.2009.06.005>, 2009.
- 766 Dhont, D. and Chorowicz, J.: Review of the neotectonics of the Eastern Turkish–Armenian Plateau by geomorphic
767 analysis of digital elevation model imagery, *International Journal of Earth Sciences*, 95, 34–49,
768 <https://doi.org/10.1007/s00531-005-0020-3>, 2006.
- 769 Ebinger, C. J., Yemane, T., Woldegabriel, G., Aronson, J. L., and Walter, R. C.: Late Eocene–Recent volcanism and
770 faulting in the southern Main Ethiopian Rift, *Journal of the Geological Society*, 150, 99–108,
771 <https://doi.org/10.1144/gsjgs.150.1.0099>, 1993.
- 772 Ebinger, C. J., Yemane, T., Harding, D. J., Tesfaye, S., Kelley S., and Rex D. C.: Rift deflection, migration, and
773 propagation: Linkage of the Ethiopian and Eastern rifts, Africa, *Geological Society of America Bulletin*,
774 112, 163–176, [https://doi.org/10.1130/0016-7606\(2000\)112<163:RDMAPL>2.0.CO;2](https://doi.org/10.1130/0016-7606(2000)112<163:RDMAPL>2.0.CO;2), 2000.
- 775 Erbello, A. and Kidane, T.: Timing of volcanism and initiation of rifting in the Omo-Turkana depression, southwest
776 Ethiopia: Evidence from paleomagnetism, *Journal of African Earth Sciences*, 139, 319-329,
777 <https://doi.org/10.1016/j.jafrearsci.2017.12.031>, 2018.
- 778 FAO, Food and Agriculture Organization, *Global Forest Resources Assessment 2000: Main Report*, FAO Forestry
779 Paper 140, Rome, Italy, [https://doi.org/10.1016/S0264-8377\(03\)00003-6](https://doi.org/10.1016/S0264-8377(03)00003-6), 2001
- 780 Fisher, P., Wood, J., and Cheng, T.: Where is Helvellyn? Fuzziness of multi-scale landscape morphometry,
781 *Transactions of the Institute of British Geographers*, 29, 106–128, <https://doi.org/10.1111/j.0020-2754.2004.00117.x>, 2004.
- 782
- 783 Fritz, H., Abdelsalam, M., Ali, K. A., Bingen, B., Collins, A. S., Fowler, A. R., Ghebreab, W., Hauzenberger, C. A.,
784 Johnson, P. R., Kusky, T. M., and Macey, P.: Orogen styles in the East African Orogen: a review of the
785 Neoproterozoic to Cambrian tectonic evolution, *Journal of African Earth Sciences*, 86, 65–106,
786 <https://doi.org/10.1016/j.jafrearsci.2013.06.004>, 2013.
- 787 Fubelli, G., Abebe, B., Dramis, F., and Vinci, S.: Geomorphological evolution and present-day processes in the
788 Dessie Graben (Wollo, Ethiopia), *Catena*, 75, 28–37, <https://doi.org/10.1016/j.catena.2008.04.001>, 2008.

789 Ganas, A., Pavlides, S., and Karastathisa, V.: DEM-based morphometry of range-front escarpments in Attica, central
790 Greece, and its relation to fault slip rates, *Geomorphology*, 65, 301–319,
791 <https://doi.org/10.1016/j.geomorph.2004.09.006>, 2005.

792 Gao, M., Zeilinger, G., Xu, X., Wang Q., and Hao, M.: DEM and GIS analysis of geomorphic indices for evaluating
793 recent uplift of the northeastern margin of the Tibetan Plateau, China, *Geomorphology*, 190, 61–72,
794 <https://doi.org/10.1016/j.geomorph.2013.02.008>, 2013.

795 Gessesse D.: Forest Decline in South Central Ethiopia Extent, history and process. Doctoral dissertation.
796 Department of Physical Geography and Quaternary Geology. Stockholm University, Sweden, 2007.

797 Gete, Z. and Hurni, H.: Implications of Land Use and Land Cover dynamics for mountain resource degradation in
798 the northwestern Ethiopian highlands, *Mountain Research and Development*, 21, 184–191,
799 [https://doi.org/10.1659/0276-4741\(2001\)021\[0184:IOLUAL\]2.0.CO;2](https://doi.org/10.1659/0276-4741(2001)021[0184:IOLUAL]2.0.CO;2), 2001.

800 Gezahegn A. and Dessie T.: Report on Engineering geophysical investigation of the Blue Nile basin for rerouting of
801 the main road, Ethiopian Institute of Geological Survey, 1994.

802 Goitom, B., Oppenheimer, C., Hammond, J. O., Grandin, R., Barnie, T., Donovan, A., Ogubazghi, G., Yohannes, E.,
803 Kibrom, G., Kendall, J. M. and Carn, S. A.: First recorded eruption of Nabro volcano, Eritrea, 2011,
804 *Bulletin of volcanology*, 77, 85, 2015.

805 Gouin, P.: Kara Kore and Serdo epicenters: relocation and tectonic implications, *Bulletin of the Geophysical*
806 *Observatory*, vol. 15, 15-25 pp., 1975.

807 Gouin, P.: Earthquake history of Ethiopia and the Horn of Africa, International Development Research Centre,
808 Ottawa, Canada, 1979.

809 Habtamu, E., Ermiyas, F., Tutan, N., and Tsigehana, T.: Engineering Geological Map of Dila Sheet at scale of
810 1:250,000 scale (NB 37-6), Geological Survey of Ethiopia, Addis Ababa, 2012.

811 Hayward, N. J. and Ebinger, C. J.: Variations in the along-axis segmentation of the Afar Rift system, *Tectonics*, 15,
812 244–257, <https://doi.org/10.1029/95TC02292>, 1996.

813 Hearn, G. J.: Slope hazards on the Ethiopian road network, *Quarterly Journal of Engineering Geology and*
814 *Hydrogeology*, 2018-2058. 2018.

815 ISRM, International Society of Rock Mechanics Commission on Testing Methods: Suggested method for
816 determining point load strength, *Int. J. Rock Mech. Min. Sci. and Geomech.*, 22, 51-60,
817 [https://doi.org/10.1016/0148-9062\(85\)92985-7](https://doi.org/10.1016/0148-9062(85)92985-7), 1985.

818 Janetos, A. C., Justice, C. O.: Land covers global productivity: a measurement strategy for the NASA programme,
819 *International Journal of Remote Sensing*, 21, 1491-1512, <https://doi.org/10.1080/014311600210281>,
820 2000.

821 JICA and GSE: The Project for Developing Countermeasures against Landslides in the Abay River Gorge, technical
822 report, Japan International Cooperation Agency and Geological Survey of Ethiopia, 348 pp., 2012.

823 Kopačková, V., Rappich, V., Šebesta, J., and Zelenkova, K.: Slope dependent morphometric analysis as a tool
824 contributing to reconstruction of volcano evolution, In *Earth and environmental sciences*, InTech,
825 <https://doi.org/10.5772/29466>, 2011.

826 Kropáček, J., Vařilová, Z., Baroň, I., Bhattacharya, A., Eberle, J., and Hochschild, V.: Remote sensing for
827 characterisation and kinematic analysis of large slope failures: Debre sina landslide, main ethiopian rift
828 escarpment, *Remote Sensing*, 7, 16183-16203, <https://doi.org/10.3390/rs71215821>, 2015.

829 Kumar, V., Gupta, V., and Sundriyal, Y. P.: Spatial interrelationship of landslides, litho-tectonics, and climate
830 regime, Satluj valley, Northwest Himalaya, *Geological Journal*, 54, 537–551,
831 <https://doi.org/10.1002/gj.3204>, 2019.

832 Kycl, P., Rappich, V., Verner, K., Novotný, J., Hroch, T., Mišurec, J., Eshetu, H., Haile, E. T., Alemayehu, L., and
833 Goslar, T.: Tectonic control of complex slope failures in the Ameka River Valley (Lower Gibe Area,
834 central Ethiopia): Implications for landslide formation, *Geomorphology*, 288, 175-187,
835 <https://doi.org/10.1016/j.geomorph.2017.03.020>, 2017.

836 Lemessa, G., Asfaw, B., Mamo, S., and Ashenafi, S.: Mass movement hazards assessment on Betto and Sawla sub
837 sheet of Goffa district, North Omo Zone, Southern Nations Nationalities and People’s Regional State,
838 technical Report, Geological Survey of Ethiopia, 2000.

839 Mancini, F., Ceppi, C., and Ritrovato, G.: GIS and statistical analysis for landslide susceptibility mapping in the
840 Daunia area, Italy, *Nat. Hazards Earth Syst. Sci.*, 10, 1851-1864, [https://doi.org/10.5194/nhess-10-1851-](https://doi.org/10.5194/nhess-10-1851-2010)
841 [2010](https://doi.org/10.5194/nhess-10-1851-2010), 2010.

842 Meinhardt, M., Fink, M., and Tünschel, H.: Landslide susceptibility analysis in central Vietnam based on an
843 incomplete landslide inventory: Comparison of a new method to calculate weighting factors by means of
844 bivariate statistics, *Geomorphology*, 234, 80-97, <https://doi.org/10.1016/j.geomorph.2014.12.042>, 2015.

845 Melese, S. M.: Effect of land use land cover changes on the forest resources of Ethiopia, *International Journal of*
846 *Natural Resource Ecology and Management*, 1, 51, <https://doi.org/10.11648/j.ijnrem.20160102.16>, 2016.

847 Muluneh, A. A., Cuffaro, M., and Doglioni, C.: Left-lateral transtension along the Ethiopian Rift and constrains on
848 the mantle-reference plate motions, *Tectonophysics*, 632, 21-31,
849 <https://doi.org/10.1016/j.tecto.2014.05.036>, 2014.

850 Peduzzi, P.: Landslides and vegetation cover in the 2005 North Pakistan earthquake: a GIS and statistical
851 quantitative approach, *Nat. Hazards Earth Syst. Sci.*, 10, 623-640, [https://doi.org/10.5194/nhess-10-623-](https://doi.org/10.5194/nhess-10-623-2010)
852 [2010](https://doi.org/10.5194/nhess-10-623-2010), 2010.

853 Pike, R. J.: Geomorphometry-diversity in quantitative surface analysis, *Progress in Physical Geography*, 24, 1-20,
854 <https://doi.org/10.1177/030913330002400101>, 2000.

855 Rapprich, V., Eshetu, H.: Geological hazards and engineering geology maps of Dilla NB 37-6, Czech Development
856 Agency, Czech Geological Survey, Geological Survey of Ethiopia, 2014.

857 Rapprich, V., Erban, V., Fárová, K., Kopačková, V., Bellon, H., and Hernandez, W.: Volcanic history of the
858 Conchagua Peninsula (eastern El Salvador), *Journal of Geosciences*, 55, 95-112,
859 <https://doi.org/10.3190/jgeosci.069>, 2010.

860 Rapprich, V., Nida, D., and Bizuye, Y.: Geological hazards and engineering geology maps of Hossana NB 37-2,
861 Czech Development Agency, Czech Geological Survey, Geological Survey of Ethiopia, 2014.

862 Saria, E., Calais, E., Stamps, D. S., Delvaux, D., and Hartnady, C. J. H.: Present-day kinematics of the East African
863 Rift, *Journal of Geophysical Research: Solid Earth*, 119, 3584-3600,
864 <https://doi.org/10.1002/2013JB010901>, 2014.

865 Sembroni, A., Faccenna, C., Becker T. W., Molin, P., and Abebe, B.: Long-term, deep-mantle support of the
866 Ethiopia-Yemen Plateau, *Tectonics*, 35, 69-488, <https://doi.org/10.1002/2015TC004000>, 2016.

867 Tadesse, T.: Recent landslide and resulting damages in the Blue Nile River Gorge and its tributaries, Eastern Gojam
868 Zone, Technical Report, Geological Survey of Ethiopia, 1993.

869 Temesgen, B., Umer, M., Asrat, A., Berakhi, O., Ayele, A., Francesco, D. and Demissie, M.: Landslide hazard on
870 the slopes of Dabicho Ridge, Wondo Genet area: the case of June 18, 1996 event, *SINET: Ethiopian*
871 *Journal of Science*, 22, 127-140, 1999

872 Temesgen, B., Mohammed, M. U., and Korme, T.: Natural hazard assessment using GIS and remote sensing
873 methods, with particular reference to the landslides in the Wondogenet area, Ethiopia, *Physics and*
874 *Chemistry of the Earth, Part C: Solar, Terrestrial & Planetary Science*, 26, 665-675,
875 [https://doi.org/10.1016/S1464-1917\(01\)00065-4](https://doi.org/10.1016/S1464-1917(01)00065-4), 2001.

876 U.S. Geological Survey, Earthquake Hazards Program, Advanced National Seismic System (ANSS),
877 Comprehensive Catalogue of Earthquake Events and Products: Various,
878 <https://doi.org/10.5066/F7MS3QZH>, 2017.

879 Vařilová, Z., Kropáček, J., Zvelebil, J., Šťastný, M. and Vilímek, V.: Reactivation of mass movements in Dessie
880 graben, the example of an active landslide area in the Ethiopian Highlands, *Landslides*, 12, 985-996,
881 <https://doi.org/10.1007/s10346-015-0613-2>, 2015.

882 Verner, K., Megerssa, L., Buriánek, D., Martínek, K., Hroch, T., Yakob, M., Haregot, A., Bewketu, H., Mosisa, A.,
883 Dalke, G., Hejtmánková, P., and Krejčí, Z.: Geological map at a scale of 1:50,000, Geological and thematic
884 maps at a scale of 1:50,000 for Mejo, Leku, Arba Minch and Dila areas, SNNPR, Ethiopia. Czech
885 Geological Survey, Prague, Map Sheet 0638-D2 Mejo, [2018a](#).

886 Verner, K., Megerssa, L., Hroch, T., Buriánek, D., Martínek, K., Yakob, M., Haregot, A., Janderková, J., Šíma, J.,
887 Kryštofová, E., Valenta, J., Bewketu, H., Mosisa, A., Dalke, G., Assefa, G., Pécskay, Z., Hejtmánková, P.,
888 and Krejčí, Z.: Explanatory notes to the thematic geoscientific maps of Ethiopia at a scale of 1:50,000,
889 Czech Geological Survey, Prague, Map Sheet 0638-D2 Mejo, [2018b](#).

890 Verner, K., Megerssa, L., Hroch, T., Buriánek, D., Martínek, K., Gebremariyam, H., Tadesse, E., Legesse, F., Nisra,
891 E., Abateneh, B., Hejtmánková, P., and Krejčí, Z.: Geological map at a scale of 1:50,000, Geological and
892 thematic maps at a scale 1:50,000 for Mejo, Leku, Arba Minch and Dila areas, SNNPR, Ethiopia, Czech
893 Geological Survey, Prague, Map Sheet 0637-D3 Arba Minch, 2018c.

894 Verner, K., Megerssa, L., Hroch, T., Buriánek, D., Martínek, K., Janderková, J., Šíma, J., Kryštofová, E.,
895 Gebremariyam, H., Tadesse, E., Legesse, F., Nisra, E., Abateneh, B., Assefa, G., Valenta, J., Pécskay, Z.,

896 Hejtmánková, P., and Krejčí, Z.: Explanatory notes to the thematic geoscientific maps of Ethiopia at a scale
897 of 1:50,000, Czech Geological Survey, Prague, Map Sheet 0637-D3 Arba Minch, 2018d.

898 Wilks, M., Ayele, A., Kendall, J. M., and Wookey, J.: The 24th January 2016 Hawassa earthquake: Implications for
899 seismic hazard in the Main Ethiopian Rift, *Journal of African Earth Sciences*, 125, 118-125,
900 <https://doi.org/10.1016/j.afrearsci.2016.11.007>, 2017.

901 Williams, F. M., Williams, M. A. J., and Aumento, F.: Tensional fissures and crustal extension rates in the northern
902 part of the Main Ethiopian Rift, *Journal of African Earth Sciences*, 38, 183-197,
903 <https://doi.org/10.1016/j.afrearsci.2003.10.007>, 2004.

904 Woldearegay, K.: Review of the occurrences and influencing factors of landslides in the highlands of Ethiopia: With
905 implications for infrastructural development, *Momona Ethiopian Journal of Science*, 5, 3-31,
906 <https://doi.org/10.4314/mejs.v5i1.85329>, 2013.

907 Woldegabriel, G., Heiken, G., White, T. D., Asfaw, B., Hart, W. K., and Renne, P. R.: Volcanism, tectonism,
908 sedimentation, and the paleoanthropological record in the Ethiopian Rift System, *Special papers-Geological*
909 *Society of America*, 83-99, 2000.

910 Wolfenden, E., Ebinger, C., Yirgu G., Deino A., Ayale D.: Evolution of the northern Main Ethiopian rift: birth of a
911 triple junction, *Earth and Planetary Science Letters*, 224, 213–228,
912 <https://doi.org/10.1016/j.epsl.2004.04.022>, 2004.

913 Wood, J. D.: The geomorphologic characterization of digital elevation models, Ph.D. Thesis, University of
914 Leicester, UK, 1996.

915 Wotchoko, P., Bardintzeff, J. M., Itiga, Z., Nkouathio, D. G., Guedjeo, C. S., Ngnoupeck, G., Dongmo, A. and
916 Wandji, P.: Geohazards (Floods and Landslides) in the Ndop Plain, Cameroon volcanic nine, *Open*
917 *Geosciences*, 8, 429-449, <https://doi.org/10.1515/geo-2016-0030>, 2016.

918 Xue, L., Alemu, T., Gani, N. D., and Abdelsalama, M. G.: Spatial and temporal variation of tectonic uplift in the
919 southeastern Ethiopian Plateau from morphotectonic analysis, *Geomorphology*, 309, 98–111,
920 <https://doi.org/10.1016/j.geomorph.2018.02.025>, 2018.

921 Yekoye, B., Yewubinesh, B., and Debebe, N.: Engineering Geological Map of Hosaina sheet (NB 37-2) at scale of
922 1:250,000, Geological Survey of Ethiopia, Addis Ababa, 2012.

923 Zvelebil, J., Šíma, J., and Vilímek, V.: Geo-risk management for developing countries—vulnerability to mass
924 wasting in the Jemma River Basin, Ethiopia, *Landslides*, 7, 99-103, <https://doi.org/10.1007/s10346-009-0191-2>, 2010.

926 Zwaan F., Schreurs G.: Rift segment interaction in orthogonal and rotational extension experiments: Implications for
927 the large-scale development of rift systems. *Journal of Structural Geology*, 140, 1-17,
928 <https://doi.org/10.1016/j.jsg.2020.104119>, 2020.

929